Theory of fluorescence excitation spectra using anharmonic-Coriolis coupling in S_1 and internal conversion to S_0 . II. Application to the channel three problem in benzene for the 14^11^2 band

Adam Helman and R. A. Marcus Arthur Amos Noyes Laboratory of Chemical Physics,^{a)} California Institute of Technology, Pasadena, California 91125

(Received 28 May 1993; accepted 24 June 1993)

Rotational lines in the fluorescence excitation spectra of the 14¹1² band of the first excited singlet state (S_1) of benzene are calculated for various J and K. For this purpose, perturbation theory is used to obtain an "eigenstate" in S_1 . Internal conversion to S_0 via Franck-Condon (FC) factors is then calculated. A search procedure is used to obtain the important contributors to this S_1 state and to this internal conversion process $S_1 \rightarrow S_0$ using the perturbation theory coefficients and the FC factors in the evaluation function. At low J, the calculated lines with K=0 are sharp, other lines being broadened and diminished in intensity. The calculated K=0 lines have a linewidth proportional to J(J+1). For high J, the lines with K=J remain sharp, the other lines being broadened and diminished in intensity. These various results are in general agreement with the experimental findings. The onset of channel three in benzene occurs in the present mechanism via anharmonic-Coriolis coupling in the S_1 state plus internal conversion to S_0 . The calculations suggest that, at low J, parallel Coriolis coupling causes mixing of the in-plane mode-excited "light state" with in-plane modes that are anharmonically coupled to out-of-plane modes. Dark states with certain excited out-of-plane mode contributions possess large FC factors for the internal conversion to S_0 . At high J, on the other hand, the in-plane modes are coupled directly to these out-of-plane modes by perpendicular Coriolis coupling. Paths involving two perpendicular Coriolis operators are important at high J in the present calculation—their matrix elements are larger at high J and so they become more competitive relative to purely anharmonic coupling operators. Such two-Coriolis paths at high J are expected to yield multiple excitation in the out-of-plane modes and further enhance the internal conversion. The perpendicular Coriolis coupling is least at J=K and so these lines survive at high J. Two-Coriolis operator paths are calculated to be relatively unimportant at low J. The present calculations, using the same electronic matrix element, account for both the low $J_{K=0}$ and high $J_{K=J}$ sets of lines being the dominant ones. Aspects regarding further study are discussed.

I. INTRODUCTION

In studies of fluorescence of the first excited singlet state (S_1) of benzene, a sudden drop in fluorescence intensity occurs for energies somewhat in excess of 3000 cm⁻¹ above the S_1 electronic origin. Historically, the unknown decay channel responsible for this cutoff has been termed "channel three," and has been a topic of experimental and theoretical research for the past 25 years. He while it was first described some time ago, he it has since been studied using high resolution one-photon has been and Doppler-free two-photon electronic spectroscopies. The latter techniques have led to rotationally resolved electronic absorption spectra of excited state benzene.

At low vibrational energies, below the onset of the channel three region and where benzene acts in the small molecule limit, it has been possible to excite various rovibronic quantum states and observe both the expected rovibrational lines and isolated avoided crossings (resonances) with other dark states. ^{7,10,19,20} These resonances reflect details of the couplings of the zeroth order states. Earlier, we treated such avoided crossings theoretically using pertur-

bation theory, in the form of the van Vleck contact transformation, employed commonly in the treatment of molecular vibration–rotation problems. The coupling terms used involved principally cubic anharmonicities and various order Coriolis terms.²³ Typically, quasiresonant states differing in four vibrational quanta were coupled by some few hundred state-to-state paths, the number depending on the states, and third order perturbation theory²⁴ was employed. In that study, the energy in excess of the zero point energy was 1570 cm⁻¹. The results were in reasonable agreement with the experiments.

At higher vibrational energies, namely in the channel three region, the rotationally resolved spectra show a loss of intensity for individual lines, indicating a fast decay process which competes successfully with the fluorescence. $^{8,10,12,14-16,22}$ Most of the individual rotational lines are then absent. For example, for the $14^{1}1^{2}$ band 25 (3412 cm⁻¹), at low values of J only the K=0 lines remain. 15,22 (For example, the $J_{K}=0_{0}$ to 14_{0} lines are depicted in Ref. 15.) Their width is dependent on the rotational quantum number J. At high values of J, only the K=J lines survive to any major extent. 15 (For example, in Ref. 15, the $J_{K}=27_{27}$ to 45_{45} lines are depicted.) Close to the threshold of

a)Contribution No. 8637.

channel three behavior, the $14^{1}1^{1}16^{2}$ state at 2963 cm⁻¹ shows at low J a more gradual fall-off intensity of lines with increasing K.¹⁵ One explanation of the channel three behavior involves internal conversion. ²⁶⁻³⁹ Another involves a postulated additional electronic state ^{40,41(a)} or possibly a chemical reaction channel. ⁴² A detailed calculation involving the molecular parameters of benzene is given here for the $S_1 \rightarrow S_0$ internal conversion (IC) mechanism, and the results are compared with the experimental data.

In the present study, the important S_1 component of the relevant eigenstate in benzene is calculated using perturbation theory containing, among others, cubic anharmonic coupling and various Coriolis interaction terms. Zeroth order states in S_1 which differ in up to nine quanta from the light state in S_1 are included as contributors. A result is then obtained for the S_0 contribution to the molecular eigenstate by using the kinetic energy operator for IC to the ground electronic state S_0 . The calculation utilizes, in addition to the perturbation theory in S_1 , an "artificial intelligence" (AI) search among the many contributing FC active states in S_1 and among the states to which they are coupled in S_0 . Fluorescence excitation spectra are then calculated and compared with experiment for the $14^{1}1^{2}$ vibronic band in S_{1} . This band, at 3412 cm⁻¹, is well within the channel three region. Rotationally resolved data for this band have been obtained mainly by Riedle, Neusser, and Schlag. 10,12,14–16,22 The present paper is an application of the treatment outlined in the previous paper (part I).43

The detailed expression contains an electronic internal conversion matrix element. The latter could either be evaluated ab initio, 44 or, as in the present paper, evaluated from the experimental slope of the plot of linewidth vs J(J+1) for the K=0 spectral lines at low J, and then used to make predictions of other properties of the system. Its value, so estimated, is then compared with an ab initio value.

In a procedure different from the present one, Dietz and Fischer used an analytical approach for IC in the $14^{1}1^{2}$ state of S_{1} benzene.³⁵ They assumed a statistical distribution of energy and an equidistant spacing of zeroth order dark states in S_{1} , coupled to the $14^{1}1^{2}$ light state, a single value for a Coriolis coupling parameter and one for a cubic anharmonic parameter. In another study, Hornburger and co-workers^{32–34} assumed a statistical distribution of the vibrational energy in S_{1} to calculate the internal conversion rates to S_{0} as a function of vibrational energy. Experimental evidence against a statistical model has been given by Yoshihara and co-workers who found that the short-time spectra (before collisional relaxation) are characteristic of the level initially selected.⁴¹

Details of the procedure specific to treating the $14^{1}1^{2}$ band of benzene are given in Sec. II. Results of the treatment of the $14^{1}1^{2}$ band are described in Sec. III, including the use of dark states in S_{1} , the rotational lines and fluorescence excitation spectra at low and at high J, and the robustness of calculated spectral lines with respect to random shifts of vibronic band origins in the S_{1} state. These features of the results are discussed in Sec. IV, where a comparison is made with experiment. A calculation of the

distribution of the importantly contributing dark states in the S_1 eigenstate is also given for comparison with a statistical model used in Refs. 32–34 and 36. Some concluding remarks are given in Sec. V.

II. PROCEDURE FOR THE 14112 S1 BAND

A. Overview

In part I, the model in which a single molecular "eigenstate" of the S_1 Born–Oppenheimer Hamiltonian is coupled via internal conversion to a quasicontinuum of S_0 rotational–vibrational states was discussed.⁴³ The S_1 eigenstate $\Psi_{S_1} = \psi_{S_1}^{\rm el} \psi_{S_1}^{\rm vr}$ can be written in terms of a linear combination of zeroth order rigid rotor harmonic oscillator (RRHO) states $\psi_{S_1,i}^{\rm vr}$

$$\psi_{S_1}^{\text{vr}} = \sum_{i} c_i \psi_{S_1, i}^{\text{vr}}.$$
 (2.1)

The c_i 's are obtained by perturbation theory, using the $|14^11^2;J,K\rangle$ "light" state as the zeroth order wave function, a state that is accessible by two-photon absorption from the S_0 ground state.

For the two-photon absorption of benzene, the experimental data leading to the 14^11^2 band are consistent with a qQ branch ($\Delta J = \Delta K = 0$) of the electronic transition. 45,46 By group-theoretic and other arguments, only the state $|14^11^2;J,K\rangle$ was a suitable candidate for the excited ("light") state, when the other background RRHO states in S_1 at an energy near the 14^11^2 band ($3412~{\rm cm}^{-1}$) were considered. 12,47

The states $|14^11^2,J,k\rangle$ are doubly degenerate. k, whose magnitude is K, may be positive or negative. Since typically these two states do not couple with each other except in high order (such coupling matrix elements are not considered here), each such state $|14^11^2;J,k\rangle$ may be considered nondegenerate for our purposes, and so we use nondegenerate perturbation theory in determining the S_1 eigenvector

For K>0 in the light state, with a single Coriolis operator (as in the low J calculations), only states with the same sign of k as the light state are available in S_1 , regardless of whether positive or negative k values are considered. Since the relevant coupling matrix elements and zeroth order energies of states differing only in the sign of k are identical, it is sufficient to consider, in the present calculations, only positive values of k for the initial state in the perturbation theory. For these states, K=k and so the magnitude K=|k| is used in the notation in this paper.

When K=0 in the light state, access to states with k=1 and k=-1 occurs via perpendicular Coriolis coupling and they are explicitly included. Since zeroth order states with k=1 and k=-1 (and k=2, -2) do not have the same energy as the initial (k=0) zeroth order state, nondegenerate perturbation theory can be used.

The wave function $|\psi_{S_1}^{\text{vr}}\rangle$ can be expressed in terms of a projection operator **P** and the unperturbed state $|14^11^2; J, K\rangle$, ⁴⁸ where

$$|\psi_{S_1}^{\text{vr}}\rangle = \mathbf{P}|14^11^2, J, K\rangle. \tag{2.2}$$

Using nondegenerate perturbation theory, the part of P operating on the $|14^11^2;J,K\rangle$ subspace is⁴⁸

$$\mathbf{P} = \mathbf{P}_0 + \frac{\mathbf{Q}_0}{a} \mathbf{V}_{\mathbf{S}_1} \mathbf{P}_0 + \frac{\mathbf{Q}_0}{a} \mathbf{V}_{\mathbf{S}_1} \frac{\mathbf{Q}_0}{a} \mathbf{V}_{\mathbf{S}_1} \mathbf{P}_0 + \cdots, \qquad (2.3)$$

where P_0 and Q_0 are projection operators

$$\mathbf{P}_0 = |\psi_{S_1,s}^{\text{vr}}\rangle\langle\psi_{S_1,s}^{\text{vr}}|,\tag{2.4}$$

$$\mathbf{Q}_0 = \sum_{j \neq s} |\psi_{S_1,j}^{\text{vr}}\rangle \langle \psi_{S_1,j}^{\text{vr}}|, \qquad (2.5)$$

and a denotes $E_s^0 - \mathbf{H}_0$. E_s^0 is the eigenvalue for the zeroth order light state in S_1 , $|14^11^2;J,K\rangle$, denoted in Eq. (2.4) by $|\psi_{S_1,s}^{\text{vr}}\rangle$. The coupling of the light state by perturbation terms V_{S_1} to a manifold of S_1 RRHO states is treated in the present paper using the vibration-rotation Hamiltonian discussed in part I.⁴³ Internal conversion couplings to S_0 are computed using the golden rule and a sum involving these zeroth order components of the S_1 eigenstate.

The nonradiative linewidth (full width at half height) Δ_{nr} due to IC is given approximately in part I, in units of $\tilde{n}=1$, by

$$\Delta_{\rm nr} \simeq \frac{2\pi}{\Delta} \sum_{i} |\mathbf{V}_{\rm IC,Si}|^2, \tag{2.6}$$

where S is the S_1 eigenstate $|\psi^{\rm vr}_{S_1}\rangle$ in Eq. (2.2) (with RRHO components $\psi_{S_1,j}^{\text{vr}}$), and i labels RRHO states in S_0 in a narrow energy range Δ centered at the energy of the zeroth order light state in S_1 . The presence of the S_0 RRHO states (instead of the S_0 eigenstates) in Eq. (2.6), and the approximate formalism leading to that aspect, are discussed in part I. In Eq. (2.6) $V_{IC,si}$ involves the nuclear kinetic energy operator

$$V_{\text{IC},Si} \simeq -\langle \psi_{S_1}^{\text{el}} | \frac{\partial}{\partial \mathbf{Q}_p} | \psi_{S_0}^{\text{el}} \rangle \langle \psi_{S_1}^{\text{vr}} | \frac{\partial}{\partial \mathbf{Q}_p} | \psi_{S_0,i}^{\text{vr}} \rangle. \tag{2.7}$$

Because it is much less important, a term involving $\partial^2/\partial \mathbf{Q}_p^2$ operating only on $\psi_{S_0,i}^{\text{vr}}$ was omitted here.⁴⁹ In Eq. (2.7), the electronic matrix element is regarded as the value in the Q-centroid approximation, 50 and the vibrational matrix element includes the usual product of FC factors (the rotational matrix element $\langle J,K|J,K\rangle$ is, of course, unity). In Eq. (2.7), the normal mode Q_p is of the proper symmetry to promote the transition to S_0 . Since S_0 is of A_{1g} symmetry and S_1 of B_{2u} symmetry, the promoting modes in the case of benzene are of b_{2u} symmetry, namely, Q_{14} and Q_{15} .⁴² For the present, the same value of the electronic matrix element is assumed for both choices of the inducing mode Q_p .

The rotational lines in the fluorescence excitation spectra under collision-free conditions are calculated as Lorentzians whose width and intensity are determined by the IC rate, the fluorescence decay rate, and ground state statistical factors. The relative intensities of the individual lines were given in part I as⁴³

$$I_{J,K}(E-E_{S_1}) = I_{J,K}L,$$
 (2.8)

where $I_{J,K}$ is the integrated relative intensity of the J_K line

$$I_{J,K} = \phi_f |c_s(J',K') C_{el} C_{vib} C_{rot}(J',K',J'',K'')|^2 (2J+1)$$

$$\times f_{\text{nuc}}(J'',K'')f_{\text{Boltz}}(J'',K''), \tag{2.9}$$

$$\phi_f = \Delta_f / (\Delta_f + \Delta_{nr}) \tag{2.10}$$

and L is a Lorentzian function

$$L = \frac{1}{2\pi} \frac{(\Delta_f + \Delta_{nr})}{(E - E_{S_s})^2 + (1/4)(\Delta_f + \Delta_{nr})^2}$$
(2.11)

which, when integrated over a "line" for a particular $S_1 J_K$ state, yields unity. In Eqs. (2.9) and (2.10), ϕ_f is the fluorescence quantum yield of the given J_K state; c_s denotes the coefficient of the zeroth order light state in the S_1 quasieigenstate $\psi_{S_1}^{\text{vr}}$; C_{el} is the electronic matrix element⁵¹ for the relevant component of the two-photon absorption (TPA) tensor from state S_0 to S_1 ; C_{vib} is the vibrational matrix element of the appropriate component of the TPA tensor⁵¹ for the transition from the ground state zero vibrational level to the 14¹1² light vibrational state;⁵¹ $|C_{\rm rot}(J',K',J'',K'')|^2$ is a weighted sum of squares of rotational matrix elements, possibly complex, for several components of the TPA tensor,⁵¹ as in Eq. (2.25) below; $f_{\text{nuc}}(J'',K'')$ is a nuclear spin statistical factor for the ground state species; $^{52-54}$ $f_{\text{Boltz}}(J'',K'')$ is the Boltzmann weighting factor for the ground state at the rotational temperature of the experiment; and Δ_f is the linewidth due to fluorescence and is, in general, small compared with Δ_{nr} in the channel three region. $[\phi_f]$ in Eq. (2.10) is typically of the order of 10^{-3} or less in that region.] E_{S_1} is the energy of the quasieigenstate in S_1 . Values of the calculated nonradiative linewidth Δ_{nr} , fluorescence quantum yield ϕ_f , and I_{LK} are given in Sec. III. The correction of Eq. (2.11) for pressure broadening Δ_n and for instrumental broadening is noted later in Sec. II D.

B. Al search algorithm for S_0 RRHO states

The "AI search" employed was a very straightforward one—states in S_1 within ± 1000 cm⁻¹ of the zeroth order J_K state (the S_1 state must have the same J and have Kwithin two of that for the zeroth order state) were selected and ordered with respect to the net number of vibrational quanta q exchanged, and with respect to the net difference in K (so determining the maximum number of perpendicular Coriolis operators in a path). Paths leading to the S_1 states were found, there being no restriction on the energies of the intermediate S_1 tier states in the search. For each such "final" state, the Franck-Condon factors to the S_0 states in a small preselected energy interval about the zeroth order state were calculated. Only the states in S_1 and S_0 which yield a preassigned value of an evaluation function (E.F.) given below were retained in the search and so contributed to Δ_{nr} . Details specific to the $14^{1}1^{2}$ band in benzene are given here. All vibrational states considered in S_1 are of ungerade parity, since only they may couple with the $14^{1}1^{2}$ state, which is of b_{2u} symmetry.

Among the "acceptor modes," 11 are considered "active" in IC (i.e., $\Delta v_n \neq 0$), namely, the modes $Q_1(a_{1g})$, $Q_4(b_{2g})$, $Q_5(b_{2g})$, $Q_6(e_{2g})$, $Q_8(e_{2g})$, $Q_{10}(e_{1g})$, $Q_{11}(a_{2u})$, $Q_{14}(b_{2u})$, $Q_{16}(e_{2u})$, $Q_{17}(e_{2u})$, and $Q_{18}(e_{1u})$. The nine remaining modes ("inactive") essentially do not change their excitation, i.e., $\Delta v_n = 0$, during internal conversion. A mode is placed on the inactive list when it yields (after a search of quasienergetic states in S_0) small overlap integrals and/or too few states in S_0 . These inactive modes and their symmetries are $Q_2(a_{1g})$, $Q_3(a_{2g})$, $Q_7(e_{2g})$, $Q_9(e_{2g})$, $Q_{12}(b_{1u})$, $Q_{13}(b_{1u})$, $Q_{15}(b_{2u})$, $Q_{19}(e_{1u})$, and $Q_{20}(e_{1u})$.

The modes Q_6 to Q_{10} and Q_{16} to Q_{20} are doubly degenerate; Q_1 is the only totally symmetric (a_{1g}) active mode and Q_2 is the only totally symmetric inactive mode. There are, in addition, ten nontotally symmetric active (NTS) modes and eight NTS inactive modes. The allowed values of Δv_n for both active and inactive acceptor modes are given in part I.⁴³

In the case of benzene, the additional restriction for degenerate modes Q_t (Q_6 – Q_{10} and Q_{16} – Q_{20})

$$\Delta l_t = 0 \tag{2.12}$$

reduces a 30-dimensional search for S_0 states to a 20-dimensional search, ⁵⁵ since for each of the ten degenerate modes, the vibrational quantum number l remains constant in proceeding from S_1 to S_0 .

Since the quantum state for all inactive modes is specified, one need not sum over these modes when searching for states in S_0 with large FC overlap to a given RRHO basis state in the S_1 eigenvector. As already noted, there were nine such modes and so the 20-dimensional search is now further reduced to an 11-dimensional search.

This 11-dimensional search in the S_0 manifold was performed for the 11 active modes. In the search, the low frequency out-of-plane mode Q_4 was restricted to having at least 24 quanta in S_0 , since otherwise, the FC factor was found to be quite small. In addition to satisfying the selection rules for individual normal modes, ⁴³ a prospective rovibronic state in the S_0 manifold was required to satisfy several additional criteria in order to be selected:

- (1) The state in S_0 should lie in a specified narrow energy range Δ centered about the S_1 energy E_{S_1} of the S_1 quasieigenstate. In practice, it is sufficient to choose as the energy center the zeroth order energy of the RRHO state in S_1 that is the dominant contributor to the S_1 eigenvector, which is the light state in the present case. The narrow range Δ in Eq. (2.6) is taken to be 0.03 cm⁻¹. The zeroth order energy is 41 502 cm⁻¹ plus the rigid rotor energy $B_e[J(J+1)-\frac{1}{2}K^2]$, 41 502 cm⁻¹ being the sum of the difference in electronic origins 38 086 cm⁻¹ plus the zeroth order vibrational energy 3416 cm⁻¹ above the zero-point energy in S_1 . 56,57 In the statistical limit, Δ_{nr} should be independent of Δ , for small Δ , and the exact placement of the energy "window" should be unimportant, since in S_0 , there is a large enough density of states with similar numbers of states and coupling strength, regardless of the precise placement of the energy center.
- (2) Symmetry criteria specific to the promoting modes should also be satisfied. In benzene, Q_{14} and Q_{15} are

the promoting modes. When Q_{14} is the promoting mode, then

$$\Delta v_{14} = \pm 1, \pm 3,...$$
 and $\Delta v_{15} = 0,$ (2.13)

since Q_{15} is inactive and since there is a $\partial/\partial \mathbf{Q}_{14}$ operator in the integrand of the mode Q_{14} overlap integral, thereby switching the even-only rule for nontotally symmetric active modes⁴³ to odd only. When Q_{15} is the promoting mode, one has, instead,

$$\Delta v_{14} = 0, \pm 2, \pm 4,...$$
 and $\Delta v_{15} = \pm 1,$ (2.14)

since mode Q_{14} is active and mode Q_{15} is subject to the odd-only rule due to the $\partial/\partial Q_{15}$ operator, and being inactive is further restricted to the smallest allowed changes in its quantum number (± 1). In the search algorithm, Q_{14} and Q_{15} are alternately allowed to be the promoting mode.

(3) A tentatively selected rovibronic state in S_0 must have a sufficiently large FC overlap integral with a dark zeroth order (RRHO) state in the S_1 eigenvector that provides access to it via IC. In the evaluation function, given below, account is also taken of the contribution c_i of the S_1 RRHO state to the S_1 "eigenstate."

Each of the above selection criteria was encoded in separate subroutines which return to a 11-fold loop if the given criterion is not satisfied. A zeroth order state in S_0 was accepted when all of the above criteria were satisfied, provided the evaluation function

$$E.F. = |c_i \langle \Psi_{S_1}^{\text{vr}} | \partial / \partial \mathbf{Q}_p | \Psi_{S_0}^{\text{vr}} \rangle|$$
 (2.15)

equaled or exceeded a specified minimum value. In the present work for $J_K=6_4$, this minimum value was chosen to be $1.0\times10^{-12}~{\rm cm}^{-1}$. In the typical case of an accepted S_0 state, the matrix element in Eq. (2.15) was $\sim1\times10^{-10}~{\rm cm}^{-1}$ and c_i was ~0.01 . Cut-off values for other J_K were determined by comparing the c_i 's for such a J_K with their corresponding values (for the same S_1 vibrational state i) when $J_K=6_4$ and adjusting the cutoff in proportion to a mean value for this ratio. ⁵⁸

The disposition of energy among the S_0 normal modes was also calculated, even though it is not needed for the observables calculated in the present paper. The results could then be compared with those predicted $^{32-36}$ from statistical type models. To obtain the energy disposition among modes, a summation over S_0 states was made, each S_0 state weighted by the product of the coefficient c_i of the S_1 RRHO state in the S_1 eigenvector that the S_0 state couples to, with the FC factor for that coupling via IC, and with the amount of energy in each mode. Specifically, in the present calculation, the fraction of vibrational energy in mode Q_k in the S_0 electronic state is

$$f_{k} = \frac{\sum_{p} \sum_{j} \sum_{i} c_{i}^{2} |\langle \Psi_{S_{1},i}^{\text{vr}} | \partial / \partial \mathbf{Q}_{p} | \Psi_{S_{0},j}^{\text{vr}} \rangle|^{2} n_{k;j} \omega_{k}}{\sum_{p} \sum_{k} \sum_{j} \sum_{i} c_{i}^{2} |\langle \Psi_{S_{1},i}^{\text{vr}} | \partial / \partial \mathbf{Q}_{p} | \Psi_{S_{0},j}^{\text{vr}} \rangle|^{2} n_{k;j} \omega_{k}}, \quad (2.16)$$

where $\Psi^{\text{vr}}_{S_1,i}$ is the *i*th S_1 RRHO state that provides access to the *j*th RRHO state in S_0 , $\Psi^{\text{vr}}_{S_0,j}$; c_i is the coefficient of this *i*th state in the S_1 quasieigenstate; and $n_{k;j}$ is the vibrational quantum number in S_0 for state *j* for mode Q_k with frequency ω_k in S_0 . The sum over *p* is over the pro-

moting modes Q_{14} and Q_{15} , as noted earlier. Data used in the evaluation of integrals in Eq. (2.7) are given in Appendix A. For notational brevity, c_i^2 is used throughout this paper, as in Eq. (2.16), instead of $|c_i^2|$. In the present paper, all matrix elements and hence all c_i are real.

C. Calculation of the S₁ "molecular eigenvector"

The S_1 RRHO states appearing in Eq. (2.1) for the S_1 eigenvector are found as perturbation corrections to the zeroth order light state $|14^11^2;J,K\rangle$ upon using the terms in the S_1 vibration–rotation Hamiltonian to couple the various zeroth order states. A discussion of the coupling is given in part I.⁴³

The vibration-rotation Hamiltonian used in the calculation of c_i , the coefficient in the S_1 eigenvector, is expanded according to the perturbation order of the vibrational and rotational operators⁵⁹⁻⁶⁵

$$\mathbf{H} = \sum_{m} \sum_{n} \lambda^{m+n-2} \mathbf{H}_{mn}. \tag{2.17}$$

Here, λ is a perturbation parameter and m and n denote the degree of vibrational and rotational operators, respectively. Specific terms in Eq. (2.17) relevant to benzene are discussed in part I.⁴³

In the algorithm that couples S_1 states by terms in the rotational-vibrational Hamiltonian equation (2.17), no energy restriction was imposed on the intermediate S_1 dark states in a path. The final S_1 dark states which directly undergo IC were restricted to a ± 1000 cm⁻¹ window. (A refinement of the present numerical procedure would include a study of imposing and varying specified limits on the energies of the selected RRHO S_1 states.)

To provide access to the vast majority of dark zeroth order states in S_1 at this excess vibrational energy (3412 cm⁻¹), an exchange of about 11 vibrational quanta would have been needed (cf. Table VIII, given later, which contains a count of S_1 states in a ± 20 cm⁻¹ window). A test for "convergence" in a practical sense was made by increasing the number of dark states used in S_1 to see if the "observable" Δ_{nr} reached some limiting value. The dark states in S_1 that were found in the calculation to provide most of the FC coupling to S_0 differed from the 14^{11}^{2} state in five or six vibrational quanta. In the final calculations, the perturbation expansion⁴⁸ was truncated in the determination of the S_1 "molecular eigenstate" Ψ_{S_1} , such that a maximum net exchange of nine vibrational quanta was allowed.

The vibrational potential energy in the Hamiltonian was expanded as a polynomial in normal coordinates. The kinetic energy has only terms quadratic in their conjugate momenta with coefficients which are constants. (Alternatively, the potential could be expanded in curvilinear coordinates.) *Ab initio* cubic curvilinear constants have been calculated for benzene^{66,67} and are equal to the corresponding cubic anharmonic constants in a normal mode (rectilinear) description, e.g., as noted in Ref. 23. While they

were obtained only for the S_0 state, the anharmonic constants are needed for S_1 and they were approximated by those in S_0 as before.²³

Individual terms in \mathbf{H} up to third order were included. [In the projection operator \mathbf{P} in Eq. (2.2), terms can occur more than once.] In the first order terms, the \mathbf{H}_{21} Coriolis operator, the centrifugal distortion operator \mathbf{H}_{12} , and the cubic anharmonicity operator \mathbf{H}_{30} were included. The *ab initio* cubic force field is employed and the calculation of other relevant molecular constants are described in Appendix A.

Second order terms in **H** used in the calculations include the Coriolis operator \mathbf{H}_{31} , a centrifugal distortion operator \mathbf{H}_{22} , and the term quadratic in vibrational angular momenta $\mathbf{p}_{\alpha}\mathbf{p}_{\beta}$, $\mathbf{H}_{40}^{\mathbf{p}_{\alpha}\mathbf{p}_{\beta}}$. The quartic anharmonicity \mathbf{H}_{40} was not included; it was unavailable at the time. ⁶⁸ The only third order term included is the Coriolis operator \mathbf{H}_{41} .

The symmetry requirements for nonzero cubic force constants in \mathbf{H}_{30} and for Coriolis coupling coefficients in \mathbf{H}_{21} are well known.³⁷ The symmetry restrictions for the higher order Coriolis terms \mathbf{H}_{31} and \mathbf{H}_{41} for benzene were derived individually and are given in Appendix B of Ref. 23. For example, the distortional coordinate in \mathbf{H}_{31} , and the two in \mathbf{H}_{41} , may be of the e_{2g} or a_{1g} irreducible representations.

When doubly degenerate modes are excited in a dark RRHO S_1 state, as in the present case, not every l substate within that vibrational parentage is coupled to the $|14^11^2;J,K\rangle$ light state. For example, there are 16 l substates of parentage $1^16^19^110^116^1$, of which only six couple with the light state $|14^11^2;J,k\rangle$ according to the selection rule⁶⁰

$$-\Delta k + \sum_{i} a_{i} \Delta l_{i} + \frac{1}{2} N \sum_{i} \Delta v_{i} = pN.$$
 (2.18)

This rule reflects conservation of the overall rovibronic symmetry with respect to a C_N operation in a radiationless transition, 69,70 the C_N operation being about the principal symmetry axis for a symmetric top (here N=6). The Eq. (2.18), p is an integer, the sum over i is over all modes belonging to b-type irreducible representations (b_{1g} , b_{2g} , etc.), and the sum over t is over degenerate modes that change their respective l_t values by Δl_t with $a_t=1$ for an e_1 -type mode (e_{1g} , e_{1u}) and $a_t=2$ for an e_2 -type mode (e_{2g} , e_{2u}), in proceeding from the light to the dark state. For a given Δk , Eq. (2.18) provides the allowed Δl 's for IVR in S_1 .

All calculations are for an initial $k \ge 0$, and so k in Eq. (2.18) could be replaced by its absolute value K, except for k=0 initially. Here, we retain the k in Eq. (2.18) since k=-1 and k=-2 can occur along a selected path (k=-2 only when paths with two perpendicular Coriolis operators are included). As an example of Eq. (2.18), for coupling to the dark states of parentage $1^16^19^110^116^1$, we have $\Delta K=0$, since $\Delta K=\pm 1$ does not satisfy Eq. (2.18) for the allowed values of Δl_t . Regardless of the virtual states that provide access to these $1^16^19^110^116^1$ states when there is at most one Coriolis operator in any "path," that operator must be a parallel Coriolis one ($\Delta K=0$). When there

are two Coriolis operators in a path, an overall change of ΔK =0 is still possible by two ΔK =0 steps, and also by two perpendicular Coriolis operators, one leading to ΔK =±1 and the other to ΔK ==1.

The RRHO energies are given by

$$E = E_{\text{vib}} + B_e[J(J+1) - \frac{1}{2}K^2],$$
 (2.19)

where $E_{\rm vib}$ denotes the vibrational energy and B_e (replacing 2 C_e in the K^2 term)⁷² is the rotational constant for one of the in-plane axes. The vibrational energy $E_{\rm vib}$ is calculated from the harmonic frequencies that appear in the combination required. In the case of the S_1 state of benzene, use of the experimental fundamental frequencies⁷³ v_i permits a calculation of the combination band origins with an accuracy of perhaps $\pm 10~{\rm cm}^{-1}$, the combination band origin having an energy slightly different from the simple sum of fundamental frequencies, 23 because of different combinations of anharmonic contributions.

The calculated vibration-rotation coupling in S_1 may depend somewhat on the exact placement of combination band origins, since differences in zeroth order energy levels enter as denominators in the perturbative expansions. The effect upon calculated spectral lines of this placement should be small if the calculation is "robust." To test this robustness, a different energy randomly chosen between +10 and -10 cm⁻¹ was added to each dark zeroth order vibrational state in S_1 . The S_1 eigenvector was recalculated using this set of randomly shifted dark state energies. Two further calculations with random shifts were performed. In each case, nonradiative linewidth, fluorescence quantum yield, and intensity at peak center were calculated for a given (J,K).

Vibrational matrix elements, including those found in Coriolis operators, typically contain factors such as $\omega_i^{1/2}$ and $\omega_j^{-1/2}$, where these ω_i 's are the harmonic frequencies. Since we use experimental frequencies instead of harmonic ones, an error is made in these terms in the calculation, but it is much smaller than other error sources.

The individual matrix elements of the vibration-rotation Hamiltonian are obtained in the usual way after factoring into vibrational and rotational matrix elements of the relevant vibrational and rotational operators. Matrix elements of vibrational operators for one- and two-dimensional harmonic oscillators are well known. For matrix elements of rotational operators J_x , J_y , and J_z , these latter are transformed to spherical tensor operators J_{\pm} , and J_0 and are evaluated in the standard way.

D. Calculation of spectra

1. Modification of Eq. (2.11) for additional broadening

In calculating the spectrum, we note that the line shape is a Voigt profile, namely, the convolution of a Gaussian instrumental shape and a Lorentzian one, the latter arising from fluorescence, nonradiative transitions, and pressure broadening. ¹⁵ L in Eq. (2.11) now becomes

$$L(\nu-\nu_0) = \frac{1}{\pi^{1/2}\Delta} \frac{\Gamma}{\pi} \int_{-\infty}^{\infty} \frac{\exp{-[(u-\nu_0)/(\Delta/2)]^2 du}}{(\nu-u)^2 + (\Gamma/2)^2}$$
(2.20)

The units of ν , Γ , and Δ are in megahertz, but now Γ has a contribution from pressure broadening Δ_p , in addition to the Δ_{nr} and Δ_f present in Eq. (2.11)

$$\Gamma = \Delta_{\rm nr} + \Delta_f + \Delta_p. \tag{2.21}$$

Equation (2.20) can be rewritten in reduced form as

$$L = \frac{1}{\pi^{1/2} \Delta} \frac{a}{\pi} \int_{-\infty}^{\infty} \frac{e^{-y^2} dy}{(x - y)^2 + a^2},$$
 (2.22)

where

$$x=2(\nu-\nu_0)/\Delta, \quad a=\Gamma/\Delta.$$
 (2.23)

For ϕ_f , the quantum yield of the given J_K state in Eq. (2.9), one still uses Eq. (2.10), since in a fluorescence excitation experiment, the total emitted fluorescence is unchanged (see below). Δ_f is 1.3 MHz and Δ_p is about 15 MHz/Torr. With the 0.44 Torr used for the low J studies in Ref. 15, Δ_p is 6.6 MHz. The high J spectrum, and also one low J spectrum, were obtained at 3.9 Torr, where the linewidth, apart from the $\Delta_{\rm nr}$ contribution, is about 60 MHz. Δ in Eq. (2.23) is $5/(\ln 2)^{1/2}$ MHz, corresponding to an instrumental Gaussian width at half-height of 5 MHz.

Several experiments suggest⁷⁵ a mechanism for the pressure broadening and lead to Eq. (2.21). In experiments on a different spectral line, Wunsch et al. 76 found that the total fluorescence of an initially excited ensemble of J_K states was pressure independent. (At longer times, the fluorescent lifetime was pressure dependent, presumably reflecting a collisional deactivation of the S_1 state as a whole.) Thus, at the times of interest here, the collisions merely redistributed the electronic excitation of these fluorescence-emitting states among other fluorescing J_K states rather than quench them as a whole. However, the linewidth of an individual J_K state varies linearly with pressure. 15,75 (The slope corresponds to a large, i.e., greater than gas kinetic, cross section. 15,75) From these results on total fluorescence and on linewidths, it can be inferred⁷⁵ that the collisional broadening of an initially excited J_K state is due to collisional conversion to other J_K states. As such, the appropriate modification of Eq. (2.11) is to include such pressure broadening via the term in Eq. (2.21). while Eqs. (2.8)-(2.10) remain unchanged.

2. Rotational factor in Eq. (2.9)

The rotational factor in Eq. (2.9) is⁵¹

$$|C_{\text{rot}}|^2 = C_0 M_0 R_0 + C_1 M_1 R_1 + C_2 M_2 R_2,$$
 (2.24)

where for the qQ branch ($\Delta J = \Delta K = 0$) of a totally symmetric ($A_{1g} \rightarrow A_{1g}$) transition involved in exciting the $14_0^11_0^2$ line, the symmetric isotropic contribution $C_0M_0R_0$ has $C_0 = 1/3$, the symmetric anisotropic contribution $C_2M_2R_2$ has $C_2 = 1/30$ for the counter-circularly polarized light used in Ref. 15 and 2/15 for the parallel polarized light used in Ref. 12.⁵¹ C_1 is zero for these two polarization combina-

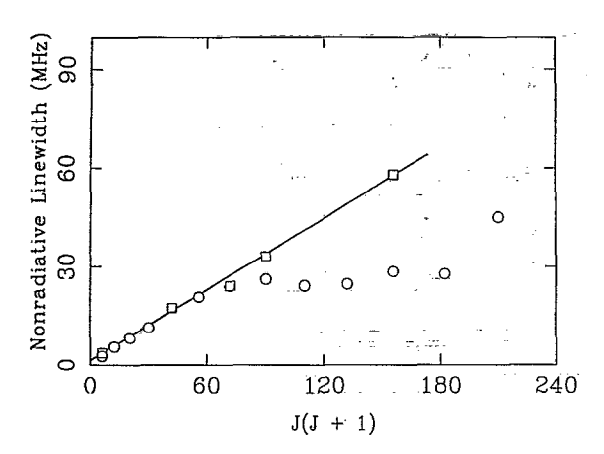


FIG. 1. Calculated linewidths (squares) at low J, plotted vs J(J+1), corresponding to excitation of eigenstates dominantly $|14^11^2;J,K\rangle$ with K=0. The experimental linewidths (circles) are included.

tions when the photons are identical in energy,⁵¹ the R's are known rotational factors, dependent on J and K, and the M's are electronic factors.⁵¹ The relative values of R_0 and R_2 reduce further the contribution of the $C_2M_2R_2$ term in Eq. (2.24), typically to only a few percent of the $C_0M_0R_0$ term,⁷⁵ and it is ignored here.

III. RESULTS FOR 14112 S. BAND

Throughout this section, the results are based on the data for $q \le 9$, where q is the net number of vibrational quanta exchanged in proceeding from the $14^{1}1^{2}$; J,K light state to dark states in S_{1} .

A. Electronic matrix element

The electronic matrix element for IC was evaluated by matching the slope of the calculated widths of the spectral lines for K=0, as a function of J(J+1), with the limiting slope at low J of the experimental K=0 plot of the total linewidth vs J(J+1). The resulting factor was used in all subsequent calculations. In both the experimental and calculated plots, the nonradiative linewidth at J=0 was negligible. In particular, in Fig. 1 the plot of the calculated linewidths of the light state are given vs J(J+1) for K=0and J=2, 6, 9, 12 (cf. Sec. III B 1) with the experimental points superimposed. The slopes of calculated and experimental results at low J match when the electronic matrix element for IC is chosen to be 3.6×10^6 cm⁻¹. As noted previously, this value was used for simplicity in the calculations, regardless of whether Q_{14} or Q_{15} was the promoting mode. (For $J_K=6_4$, about 60% to 65% of Δ_{nr} was calculated to be due to Q_{14} , given such an approximation.) The experimental and calculated intercepts in Fig. 1 are both very small (≤ 2 and 1.6 MHz, respectively).

The material presented below is based on the above value for the electronic matrix element in IC. If more contributions to $\Delta_{\rm nr}$ were used, arising from higher q or higher order anharmonicities, e.g., the magnitude of the electronic factor needed for agreement of the low J $\Delta_{\rm nr}$ vs J(J+1) plot would be smaller.

TABLE I. Calculated nonradiative linewidth Δ_{nr} , integrated line intensity $I_{J,K}$, and the coefficient squared of the light state in the S_1 eigenvector for various low J states.^a

J_K	Δ_{nr} (MHz)	$I_{J,K}$	c_s^2	Δ _{nr} (MHz) [Eq. (B1)]
. O ₀	1.6	0.72	1.00	1.6
20	3.6	2.7	1.00	3.7
2 ₀ 6 ₀	17	2.9	0.99	17
61	26	1.7	0.99	28
62	52	0.78	0.98	53
64	150	0.28	0.94	140
6 ₄ 6 ₆	150 300	0.15	0.90	280
90	33	1.2	.0.98	34
120	58	1.8	0.97	58
122	95	0.76	0.96	94
126	330	0.23	0.89	320
1212	1100	0.05	0.74	1100

 $^{{}^{}a}I_{J,K}$ denotes relative peak area (relative integrated line intensity) and is given by Eq. (2.9).

B. Calculated linewidths $\Delta_{\rm nr},$ quantum yields $\phi_f,$ and peak areas $I_{J,K}$

1. Low J

For purposes of calculating the fluorescence excitation spectrum, calculations were first made of the nonradiative linewidths Δ_{nr} for selected points. The values of J=6 and J=12 were selected as typical for low J, and the calculations were performed for different K, namely, K=0, 1, 2, 4, and 6 for J=6; and K=0, 2, 6, and 12 for J=12. The values K=0 and $K\neq 0$ correspond to the absence and presence of parallel Coriolis coupling, respectively. The results for Δ_{nr} for the above J_K states are given in Table I, based on coupling to dark S_1 states differing from the $14^{1}1^{2}$ light state in up to nine vibrational quanta. Also listed are the coefficients c_s^2 of the light state in the normalized S_1 molecular eigenvector. In Fig. 2, the calculated linewidths Δ_{nr} of the K>0 states at low J are plotted vs K for J=6 and J=12, and compared with the values obtained from the interpolation formula (B1) in Appendix B. A comparison with Eq. (B1) is given in Table I for all points.

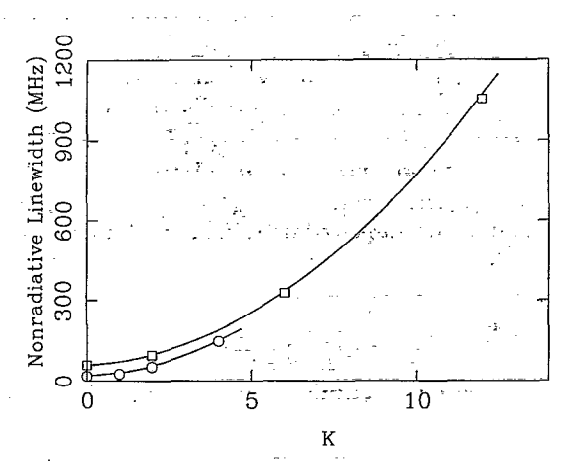


FIG. 2. Calculated linewidths at low J, plotted vs K for J=6 (circles) and for J=12 (squares). A comparison is given with the linewidths (solid lines) obtained using interpolation formula (B1).

TABLE II. Calculated nonradiative linewidth Δ_{nr} , integrated line intensity $I_{J,K}$, and the squared coefficient of the light state in the S_1 eigenvector for states with J=42, 36, and 30.^a

J_K	$\Delta_{\rm nr}$ (MHz) $\times 10^{-2}$	$I_{J,K}$	c_s^2	$\Delta_{nr} (MHz) \times 10^{-2}$ [Eqs (B2)-(B3)]
4242	2.1	1.0	0.99	2.2
4241	5.8	0.24	0.96	6.4
4240	7.9	0.13	0.94	7.8
4238	14	0.07	0.90	13
4235	31	0.03	0.79	29
4232	53	0.01	0.68	53
36 ₃₆	2.0	.1.3	0.99	1.8
36 ₃₅	4.4	0.34	0.98	4.6
3634	6.3	0.19	0.96	5.6
3632	9.5	0.11	0.93	9.4
36 ₂₉	21	0.05	0.86	20
36 ₂₆	33	0.02	0.80	36
3030	1.4	1.6	0.99	1.5
3029	2.6	0.54	0.98	3.2
30 ₂₈	3.6	0.32	0.97	3.8
30 ₂₆	7.4	0.15	0.95	6.1
30 ₂₃	13	0.09	0.91	12
3020	22	0.04	0.86	22
304	18	0.04	0.81	•••
301	17	0.05	0.82	•••
30 ₀	19	0.03	0.80	•••

 $^{{}^{}a}I_{J,K}$ denotes relative peak area (relative integrated line intensity) and is given by Eq. (2.9).

These (J,K) lines in the spectrum were given quantum yields ϕ_f obtained from Eq. (2.10). A value of Δ_f =1.3 MHz was used in all calculations.¹⁵ Values of $I_{J,K}$ were then obtained from Eq. (2.9) by introducing the nuclear spin statistics^{52–54} and Boltzmann factors. The resulting values of ϕ_f and $I_{J,K}$ are given in Table I.

2. High J

Calculations were made for $\Delta_{\rm nr}$, ϕ_f , and $I_{J,K}$; when J=30 for K=30, 29, 28, 26, 23, and 20; for $J_K=36_{36}$, 36_{35} , 36_{34} , 36_{32} , 36_{29} , and 36_{26} ; and for $J_K=42_{42}$, 42_{41} , 42_{40} , 42_{38} , 42_{35} , and 42_{32} , these values being typical at high J. (Values of K were selected such that J-K=0, 1, 2, 4, 7, and 10.) The results are given in Table II. The rotational temperature was 293 K. Calculations of $\Delta_{\rm nr}$, ϕ_f , and $I_{J,K}$ were also made when J=30, but for low K, namely, for $J_K=30_0$, 30_1 , and 30_4 , and are given in Table II.

In Fig. 3, the calculated nonradiative linewidths $\Delta_{\rm nr}$ at high J are plotted vs (J-K) for J=30, 36, and 42. The solid curves are obtained from an interpolation formula in Appendix B. The results for $\Delta_{\rm nr}$ (cale) for all points at high J and K are compared in Table II with those obtained from the interpolation formulas (B2) and (B3) in Appendix B. The states 30_0 , 30_1 , and 30_4 were not used in this interpolation.

C. Fluorescence excitation lines and spectra

The appearance of the Doppler-free two-photon spectra of the $14^{1}1^{2}$ band $^{10,12,14-16}$ is qualitatively different for the two sets of experimental conditions low J and high J. The prepared states, dominantly $|14^{1}1^{2},J,K\rangle$ in parentage,

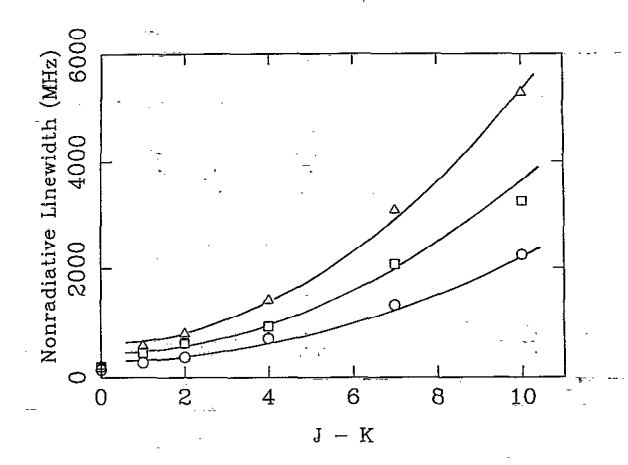


FIG. 3. Calculated linewidths at high J, plotted vs (J-K), for J=30, 36, and 42 (circles, squares, and triangles, respectively). A comparison is given with the linewidths (solid lines) obtained using interpolation formulas (B2)-(B3).

had $0 \le J \le 14$ in the data given at low J, $^{12,14-16}$ while J is typically 27 to 45 in the results at high J. The study was made at room temperature. The low J and high J cases are considered separately. These spectra occupy the 0 to -60 and -100 to -270 GHz (relative to the 0_0 line) 77 regions of the qQ branch of the fluorescence excitation spectrum, respectively. The several lines in the intervening region of -60 to -100 GHz remain to be assigned.

1. Low J

The line positions in the spectrum were calculated based on a symmetric top rigid rotor model in both the ground and excited electronic states, with a change in rotational constants ($B_{S_0} - B_{S_1}$) of 0.189 80–0.18 108 =0.00872 cm⁻¹. ^{12,14,15} The rotational temperature assumed for all studies is 293 K, all experiments having been performed at room temperature.

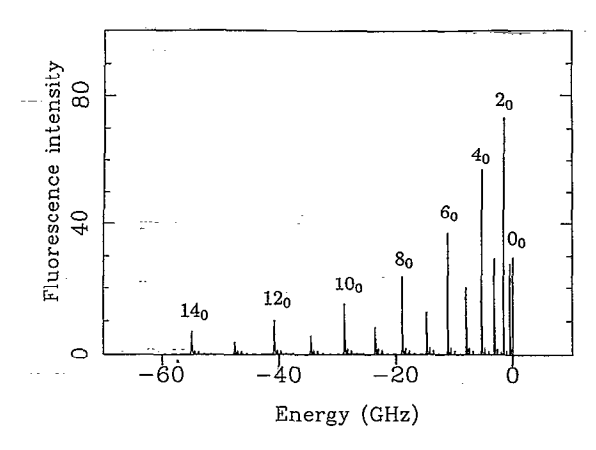


FIG. 4. The calculated 14^11^2 fluorescence excitation spectrum for the near blue edge (0 to -60 GHz) of the Q_q branch relevant for low values of J, corresponding to an experimental pressure of 0.44 Torr, with $q \le 9$. The ordinate is in arbitrary units, but are the same in all calculated spectra (Figs. 4–7, 9, and 10).

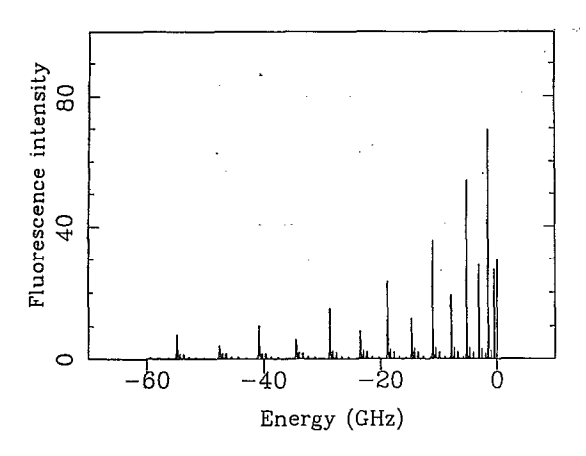


FIG. 5. The calculated 14¹1² fluorescence excitation spectrum for the near blue edge of the Q_a branch relevant for low values of J corresponding to an experimental pressure of 0.44 Torr, but with $q \le 6$.

The calculated spectral lines result from the convolution in Eq. (2.20). The value of L in Eq. (2.20) when integrated over a J_K line is unity, and so the integrated relative intensity of that line is given by I_{LK} in Eqs. (2.9) and (2.10). In the plots of the spectra, Eqs. (2.21)–(2.23)are used, in conjunction with Eqs. (2.8)-(2.10), with the Δ_p appropriate to the pressure employed.

The resulting calculated fluorescence excitation spectrum for low J is given in Fig. 4, using the interpolation for Δ_{nr} described in Appendix B, and from it, ϕ_f and I_{JK} . For comparison, the same result is given, but for $q \le 6$, in Fig. 5. Both Figs. 4 and 5 correspond to an experimental pressure of 0.44 Torr, at which the linewidth contribution due to pressure broadening is about 6 MHz. In Fig. 6, the calculated spectrum at low J for the higher pressure of 3.9 Torr is given, the contribution to the width due to pressure broadening now being about 60 MHz. The "bin" sizes used in generating the spectra, corresponding to those used in the experimental recording, are noted in Ref. 78.

In Fig. 7, a "stick spectrum" is given, namely, a plot of the integrated intensity of each line $I_{J,K}$ calculated from Eqs. (2.9) and (2.10). For comparison with the intensities,

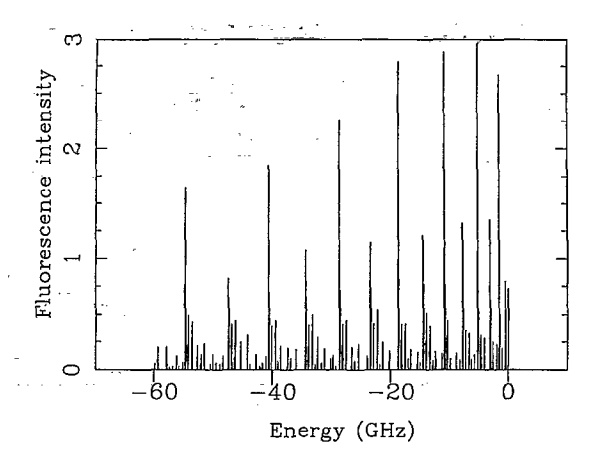


FIG. 7. The calculated 14¹1² stick spectrum, i.e., the integrated line intensities I_{LK} , for the near blue edge of the Q_a branch relevant for low values of J.

the rotational/spin statistics weighting factors for J_K states with $0 \le J \le 15$ for K=0, and with $27 \le J \le 45$ for K=J, at a rotational temperature of 20 °C are shown in Fig. 8.

2. High J

The calculated spectrum for $J_{K=J}$ =27-45 is given in Fig. 9, using a pressure of 3.9 Torr. This spectrum was based on a (J,K)-dependent fluorescence quantum yield obtained using the interpolation formulas (B2) and (B3) for Δ_{nr} in Appendix B, mentioned earlier. One interpolation formula (B2) is used for J=K and one [Eq. (B3)] for $J \neq K$, since the transitions at J = K are "one sided," i.e., only a negative ΔK can occur, while for $J \neq K$, both positive and negative ΔK is possible. (At low J, when K=0, all transitions were "two sided.") The stick spectrum for the relative integrated intensities $I_{J,K}$ of each line, based on Eqs. (2.9) and (2.10), is given in Fig. 10.

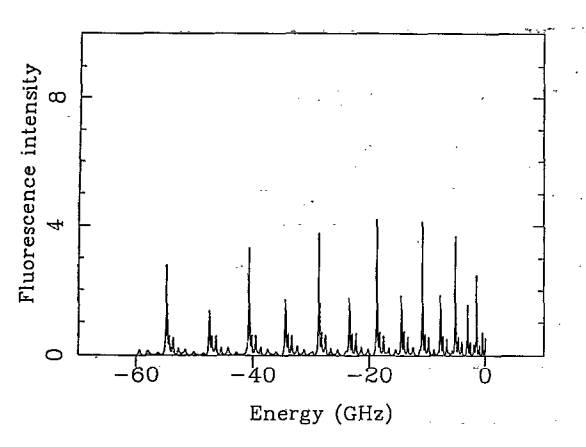


FIG. 6. The calculated 14112 fluorescence excitation spectrum for the near blue edge of the Q_a branch relevant for low values of J corresponding to an experimental pressure of 3.9 Torr with $q \le 9$.

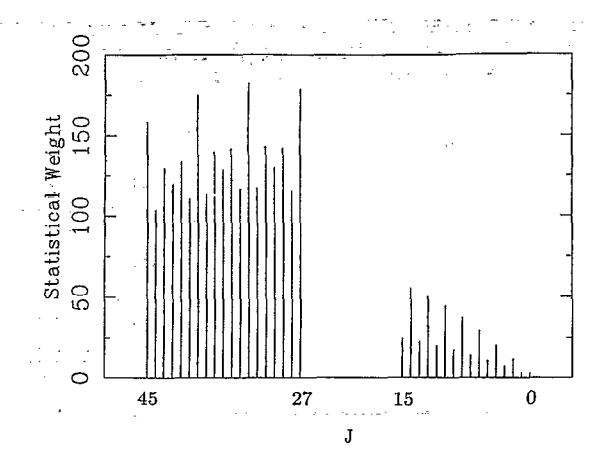


FIG. 8. Rotational/spin statistics factors at low J (0 $\leq J \leq$ 15) for K=0lines and at high J (27 $\leq J \leq 45$) for K=J lines. The temperature is 293 K.

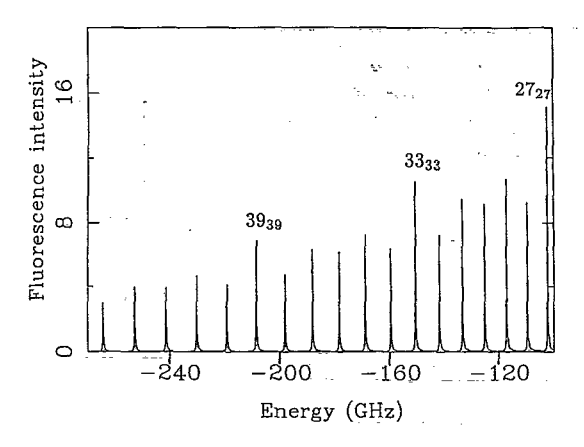


FIG. 9. The calculated fluorescence excitation spectrum for the red portion (-100 to -270 GHz) of the Q_q branch relevant for the high values of J at 293 K and a pressure of 3.9 Torr.

D. Results on particular aspects of the calculations

1. Number of Coriolis operators at low J and at high J

The contributions of paths containing different numbers of Coriolis operators (with the remaining anharmonic operators providing the exchange of vibrational quanta) were investigated at both low and at high J. For low J, the contributions to the nonradiative linewidth of paths containing zero (purely anharmonic) and one Coriolis operators are given in Table III for the $J_K=6_4$ state. The same paths there have been categorized according to q, the number of vibrational quanta exchanged, and according to the perturbation order (\mathbf{H}_{n1}) and type (parallel, perpendicular) of the Coriolis operator. All results are for $q \leq 9$. The contributions of two-Coriolis paths to the nonradiative linewidth for the 6_4 state are given in Table IV. They contribute only about 15% of the total nonradiative linewidth.

The linewidth contains a small calculated contribution (≈ 0.4 MHz) from direct IC to S_0 from the light state $|14^11^2;6,4\rangle$, i.e., without involving other S_1 states. The contribution due to paths with only cubic anharmonic op-

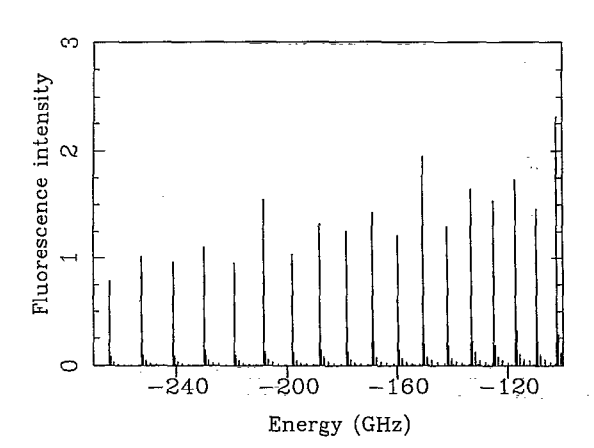


FIG. 10. The calculated stick spectrum, i.e., the integrated line intensities $I_{J,K}$, for the red portion of the Q_q branch relevant for the high values of J at 293 K.

TABLE III. Contributions to the nonradiative linewidth Δ_{nr} of purely anharmonic and of different types of Coriolis paths for $J_K=6_4$.

q^{b}	H ₃₀	Coriolis type ^c	H ₂₁	H ₃₁	H ₄₁
3 ^d	0.25		0.30	.0.65	0.59
		Ï	0.027	0.05	0.06
4	0.30	lj	1.3	1.9	2.4
		Ϊ	0.15	0.20	0.26
5	0.12	∥ '	7.6	4.5	9.2
,		Ï	. 0.9	0.6	1.2
6	0.08	li li	15.7	4.6	9.3
		Ï	2.7	0.8	1.9
7	0.06	- II	12.8	. 3.3	6.2
5.27		Ï	1.1	0.7	0.6
. 8	0.04	· ·	10.1	2.3	4.2
		Ï	0.5	0.4	0.3
9	0.03	11	8.0	1.7	3.1
		Ϊ	0.3	0.2	0.2

^aPaths may involve cubic anharmonic operators with and without a single parallel or perpendicular Coriolis operator. Values of Δ_{nr} are in megahertz.

TABLE IV. Contribution of paths with two Coriolis operators to the nonradiative linewidth for $J_K=6_4$.

\overline{q}	Type ^b	H ₂₁ H ₂₁	H ₂₁ H ₃₁	H ₂₁ H ₄₁ ^c	H ₃₁ H ₃₁ ^c	H ₃₁ H ₄₁ ^c	H ₄₁ H ₄₁ ^c
3	,	0.02	0.04	1.01			
	ij,Ï	0.02	0.01				
	⊥,∥	d	0.01				
	ı,ı	0.01	0.01				
4	,	0.11	0.17	0.07	0.07		
	⊥, ∥	0.07	0.03	.0.05	0.05		
	⊥ ,∥	d	0.04	0.03	d		
	١, ١	0.04	0.06	0.02	0.03		
5	,	0.45	0.37	0.18	0.23	0.20	
	⊥, ∥	0.36	0.23	0.17	0.18	0.09	
	⊥ ,∥	d	0.15	0.10	d	0.14	
	1,1	0.10	0.06	0.06	0.09	0.04	
6 .	. ,	0.58	0.61	0.48	0.31	0.23	0.37
-	,,_	0.68	0.05	0.80	0.60	0.42	0.52
	⊥ ,∥	d	0.04	0.66	d	0.64	d
	⊥,⊥	. 0.09	0.14	0.11	0.08	0.09	0.12
7	,	0.50	0.41	0.43	0.44	0.32	0.29
	⊥, ∥	0.53	0.37	0.63	0.32	0.45	0.42
	⊥ ,∥	d	0.28	. 0.48	d	0.46	d
	Т,1	0.10	0.08	0.08	0.06	0.06	0.09

^aValues of Δ_{nr} are given for different q and combinations (parallel, perpendicular) of Coriolis operators of different orders (H₂₁, H₃₁, H₄₁). Values are in megahertz.

 $^{{}^{\}mathrm{b}}q$ is the number of vibrational quanta exchanged.

 $^{^{\}mathrm{c}}\parallel$ and \perp represent paths with one Coriolis operator of the type indicated.

^dThese values include q < 3 as well.

bll and 1 represent Coriolis operators of the type indicated. The first symbol represents the first Coriolis operator listed in the column heading and similarly for the second symbol. When the two Coriolis operators are different, their order of occurrence in a path is not implied by their order of listing, e.g., H₂₁H₃₁ includes paths in which H₃₁ occurs first.

^cA space is blank when the given combinations of operators do not occur in paths with the given value of q [cf. Eq. (2.18)].

^dBy symmetry, the value for \bot , \parallel equals that for \parallel , \bot . Their sum is listed under \parallel , \bot .

TABLE V. Contributions to the nonradiative linewidth Δ_{nr} of paths containing different numbers and types of Coriolis operators for high J for various J_K states.*

Path type ^b	30 ₃₀	3026	3020
0	1.1	0.9	0.8
I	74	85	. 87
1	5.5	69	220
/	40	43	46
/1 °	8.7	110	310
T / c	14	120	260
1 /1	1.3	270	1300

^aValues are in megahertz and have been rounded off to two significant figures. The results are for $q \le 9$.

erators is 1.1 MHz. The net calculated value of 1.5 MHz is close to the observed value for the $J_K=0_0$ state, obtained from the lifetime data. The latter gave ≤ 2.9 MHz, which, on subtracting a $\Delta_f=1.3$ MHz, yields Δ_{nr} of ≤ 1.6 MHz. The 0_0 state cannot couple to other states in S_1 via Coriolis terms, and hence should and does have a calculated value for Δ_{nr} (≤ 1.6) MHz, which is roughly the same as the above calculated 1.5 MHz.

At high J, the contributions of paths containing zero, one and two Coriolis operators of various types are given in Table V for the $J_K=30_{30}$, 30_{26} , and 30_{20} states. The dominance of the two-Coriolis paths at high J is clear from this table. Furthermore, in the plot in Fig. 3 of $\Delta_{\rm nr}$ vs J-K, the nonlinear behavior expected from the importance of two-perpendicular Coriolis paths is evident (cf. the discussion in Sec. IV D 3).

In virtue of Eqs. (2.1)–(2.5) and (2.18), a given dark state may couple via one Coriolis operator to 14¹1² by different paths, each path involving a single parallel or a single perpendicular Coriolis operator.⁷¹ However, different one-Coriolis operator paths to a given dark state will all have the same type of single Coriolis operator, be it parallel or perpendicular.

The utility of the path analysis in Tables IV and V, and that in a subsequent paper, depends on the absence of any major quantum interference between the various paths leading to the same dark S_1 state. Only in such a case is it meaningful to speak of contributions from the individual mechanistic paths. The nonradiative linewidth Δ_{nr} is then a sum of fractional linewidth contributions from individual paths. Specifically, c_i , the coefficient of the *i*th dark S_1 state in the S_1 eigenstate, is a sum over the paths or over classes of paths, labeled by p, leading to it from the light state $c_i = \sum_p c_{i,p}$. Since the nonradiative linewidth is a sum over i with contributions proportional to the square of the coupling matrix elements, we have

TABLE VI. The number of vibrational states n_q differing in principal vibrational quantum numbers and contributions to Δ_{nr} of S_1 dark states within $\pm 20~{\rm cm}^{-1}$ of the $J_K=6_4$ light state.^a

q	n_q	Δ_{nr}	q	n_q	$\Delta_{n_{I}}$
2	0		8	59	8.8
. 3	0		9	62	7.0
4	6		10	43	
5	9	19.0	11	31	
6	25	27.7	12	14	
7	34	12.1	13	8	
		-	14	4	
			15	1	

^aBand origins are within ± 20 cm⁻¹ of the 14^11^2 band origin. n_q is listed as a function of number of vibrational quanta q by which these bands differ from 14^11^2 . Values of Δ_{nr} are in megahertz and represent the contribution from these different sets of states.

$$\Delta_{\text{nr}} = C \sum_{i,j} c_i^2 (\text{FC})_{i,j} = C \sum_{i,j,p} (c_{i,p}^2 + \text{cross terms}) (\text{FC})_{i,j},$$
(3.1)

the cross terms being $c_{i,p}c_{i,p'}$, $p'\neq p$, C being a constant. In Eq. (3.1), (FC)_{i,j} is the Franck-Condon factor for IC coupling from the S_1 dark state i to the S_0 state j.

In Tables III and V, the sum of fractional contributions to the nonradiative linewidth from different path types is nearly identical to the total nonradiative linewidth for the $J_K=6_4$ (Table III) and $J_K=30_{26}$ (Table V) states. The sums are 149 MHz for $J_K=6_4$ and 699 MHz for $J_K=30_{26}$, compared with $\Delta_{\rm nr}$ for these states of 150 and 706 MHz, respectively.

2. Number of vibrational quanta exchanged in S₁

To explore the relative contributions to the width $\Delta_{\rm nr}$ arising from S_1 final dark states differing from the 14^11^2 state by various q, the final dark states in S_1 differing in their vibrational principal quantum numbers (i.e., not counting l substrates) within ± 20 cm⁻¹ of $14^{1}1^{2}$ were counted, a sufficient number of states being in this range to be indicative of the manifold of S_1 states as a whole.⁷⁹ In the actual calculations of Δ_{nr} , however, no such restriction of S_1 energies to $\pm 20 \text{ cm}^{-1}$ was actually made. This count of states for the $J_K = 6_4$ light state and their contribution to Δ_{nr} are given in Table VI, the states considered being those of ungerade parity since, as noted earlier, only they may couple with the $14^{1}1^{2}$ zeroth order state of b_{2u} symmetry. There are (including 14¹1²) 297 states which differ in their vibrational principal quantum numbers and are in the ± 20 cm⁻¹ interval. Including l substates, the total density of vibrational band states of ungerade parity is about 85 per cm⁻¹. The calculations of Δ_{nr} in the previous sections were limited to q equal to or less than nine, due in part to computer time, since the number of paths searched rises rapidly with q. To have included states with q=10 and q=11 using the present procedure would have taken an estimated ten- or 20-fold increase in central processing unit (CPU) time. In Table VI, the largest contributions to Δ_{nr} arise from q=5 and 6.

b0 indicates paths with only cubic anharmonic coupling. ∥ and ⊥ represent paths with one Coriolis operator of the type indicated. The final four rows are for paths with the indicated combinations of two Coriolis operators.

^eThe first symbol represents the first Coriolis operator that acts in a path starting at the light state and proceeding to the dark background state in S_1 .

TABLE VII. The effect of the shift in S_1 vibrational band origins upon calculated spectral properties for $J_K=6_0$, 6_1 , 6_4 .

J_K	60	61	64
Δ _{nr} (MHz)	17	26	150
ш	16	27	150
	17	28	140
$I_{J,K}$	2.9	1.7	0.28
J,IX	3.1	1.7	0.29
	2.9	1.6	0,30
c_s^2	0.99	0.99	0.94
•	0.99	0.99	0.94
	0.99	0.99	0.93

^aThe first of three values employs the unshifted set of vibrational band origins. The second and third values employ band origins obtained as described in the text.

3. The effect of random shifts in S_1 vibronic band origins

a. The effect on Δ_{nr} . At low J, the effect of random shifts in vibrational energies on Δ_{nr} , $I_{J,K}$, and c_s^2 was calculated for the choices of $J_K=6_0$, 6_1 , and 6_4 and for 2_0 and 12_0 with q < 9. These results are given in Tables VII and VIII, respectively. The effect at high J of such random shifts for $J_K=30_{30}$, 30_{26} , and 30_{20} is given in Table IX.

b. The effect on estimated electronic matrix element. The magnitudes of the electronic matrix element for IC, required to match the observed linewidth dependence of the K=0 spectral lines on J(J+1) for the three sets of vibrational origins (one original set and two randomly shifted sets), are 3.6, 3.7, and 3.5×10^6 cm⁻¹ for $q\leqslant9$.

4. Alternative coupling terms

In addition to the nuclear kinetic energy operator, there is the rotationally dependent nonadiabatic coupling operator $\mu_{\alpha\beta}\mathbf{J}_{\alpha}\mathbf{p}_{\beta}$ that couples the S_1 and S_0 states, where \mathbf{p}_{β} is a vibrational angular momentum. Due to the inverse moment of inertia present in μ , these coupling terms are typically three orders of magnitude smaller than those obtained using the nuclear kinetic energy operator³⁰ and are not considered further. In a calculation of the number of paths, given with the next paper of this series, the number of paths by this route to states in S_0 is not significantly larger than in the present calculations that implicate Coriolis coupling in S_1 to model the experimental observations.⁸⁰

E. Energy deposition in S_0

The modes considered active or inactive in IC were given earlier in Sec. II B. The percentage of vibrational energy residing initially in the dominant accepting modes in S_0 for various values of J and K, calculated using Eq. (2.16), is listed in Table X.

IV. DISCUSSION OF RESULTS

A. A comparison of calculated and experimental fluorescence excitation spectra

We first note that experimental linewidths γ measured spectroscopically agree with those measured from time-resolved data using $\gamma = 1/2\pi\tau$, τ being the time for signal decay to 1/e of its initial intensity. Accordingly, it follows that the lines are homogeneously broadened. The present model of a discrete S_1 "eigenstate" in an S_0 continuum requires such homogeneity and is supported by the arguments given in Ref. 16 and amplified later in Sec. IV C.

1. Electronic matrix element for internal conversion

The plot of calculated linewidth vs J(J+1) when K=0, given in Fig. 1, is linear in J(J+1). The experimental linewidth for the K=0 lines, also given in Fig. 1, is similarly linear in J(J+1), but only for J<10.15

The magnitude of the electronic matrix element in IC required to match the experimental slope of linewidth vs J(J+1) (K=0), 3.6×10^6 cm⁻¹, is in reasonable agreement with the *ab initio* value of $\approx10^7$ cm⁻¹ estimated many years ago by Albrecht.⁴⁴

2. Low J

The experimental fluorescence excitation spectrum at low J (0–14) displays few rotational lines, compared with the same region of the qQ rotational branch for excitation below the channel three region. ${}^{10,12,14-16}$ Examples of the latter are the 14^1 band an excess vibrational energy of $1570 \, \mathrm{cm}^{-1}$ and the 14^11^1 band at 2493 cm⁻¹. The residual low J lines in the 14^11^2 spectra were all assigned by Neusser et al. as having K=0. 10,12,15 These authors also implicated Coriolis coupling to dark states to explain their data. 10,12

The results at low J in Table I for $\Delta_{\rm nr}$ and $I_{J,K}$ were calculated using up to and including two parallel Coriolis coupling operators and enough vibrational operators to yield a net exchange of up to and including nine vibrational quanta ($q \le 9$) in S_1 . The results (Table I and Fig. 4) may be compared with the experimental finding at low J that only the K=0 lines are observed. With parallel Coriolis coupling in the S_1 state, it is seen in Table I that the vibration—rotation coupling for $K\neq 0$ is so extensive that the calculated nonradiative linewidths $\Delta_{\rm nr}$ and fluorescence quantum yields ϕ_f tend to lead to "washed out" (broadened and weakened) spectral peaks with increasing K.

When K=0, the parallel rovibrational Coriolis coupling is absent and the pure anharmonic and perpendicular Coriolis coupling alone provides access to dark states in the S_1 manifold, as noted above, and as reflected in the proportionality of Δ_{nr} to J(J+1) in Fig. 1. [For K=0, the square of a perpendicular Coriolis matrix element is proportional to J(J+1).¹⁵] The IC from those K=0 states to S_0 still competes successfully with fluorescence from the $|14^11^2,J,K\rangle$ light state, a result evident from the low values of both the experimental¹⁴ and the calculated ϕ_f for these states. (It may also be noted that internal conversion at

these energies is reported to be comparable to or greater than the competing process of intersystem crossing to a triplet state.⁸¹) However, the calculated linewidths when K=0 are small enough, and the intensity maximum large enough, that the residual K=0 rotational lines are sharp and observable.

The square of the matrix element for parallel Coriolis coupling is proportional to K^2 , so explaining the term for $\Delta_{\rm nr}$ dependent quadratically on K^2 in Eq. (B1). The $J_K = 0_0$ state has no Coriolis coupling to dark states in S_1 , and the experimental nonradiative linewidth $\Delta_{\rm nr}$ from this state, obtained from time-resolved data, ¹⁶ was only ≤ 2 MHz, as noted earlier (Sec. III B 1). The present calculations give $\Delta_{\rm nr}$ for the 0_0 rotational state of 1.6 MHz. These values are one to several orders of magnitude smaller than typical widths for the other lines in Table I.

Our electronic matrix element, it will be recalled, was chosen to match the experimental K=0 linewidth dependence on J(J+1). Since the intercept of that plot is negligible, the present calculated ϕ_f values for K=0 at various Is should, and do, agree well with the experimental values at low J. Taking, thereby, Δ_{nr} from 0_0 to be approximately zero, an experimental ϕ_f for each K=0 state for various J's can be extracted from the time-resolved data by taking the ratio of the lifetime for the 0_0 state (or that for the lifetime of a state below the channel three region) to that for the K=0 states. In the present calculations, on the average $\phi_f \approx 10^{-2}$ for K=0 and 10^{-3} for K>0, as can be seen from the Δ_{nr} 's in Table I. In an earlier study, the experimental vibrationally, but not rotationally resolved ϕ_f was about 10⁻³ at the energy of the 14¹1² band, ¹⁴ and there the majority of rotational states had K>0.

In the calculated low J spectrum in Fig. 4, the K=0 lines dominate, with an alternating intensity (J even, J odd) due to nuclear spin statistical weights. The present calculated and observed spectra are qualitatively similar. When $q \le 6$ was used in the calculation, the resulting spectrum (Fig. 5) contains small peaks with K=1 lying toward the origin of the corresponding stronger K=0 lines. The experimental spectrum at low J does not contain these additional peaks. Thereby, the desirability of including several (up to and including nine) vibrational quanta exchanged in S_1 is clear. The experimental spectra rotational

TABLE VIII. The effect of the shift in S_1 vibrational band origins upon calculated spectral properties for $J_K=2_0$, 9_0 , 12_0 .^a

J_K	20	90	120
Δ _{nr} (MHz)	3.6	33	. 58
	3.7	32	56
	3.9	34	58
$I_{J,K}$	2.7	1.2	1.8
.,	2.6	1.2	1.9
	2.5	1.2	1.8
c_s^2	1.00	0.98	0.97
	1.00	0.98	0.97
	1.00	0.98	0.97

^aCf. footnote a of Table VII.

TABLE IX. The effect of the shift in S_1 vibrational band origins upon calculated spectral properties for $J_K=30_{30}$, 30_{20} , 30_{20} .

J_K	30 ₃₀	30 ₂₆	3020
Δ _{nr} (MHz)	140	740	2200
	135	760	2150
., .	145	730	2250
$I_{J.K}$	1.6	0.15	0.04
*,	1.7	0.14	0.04
	1.6	0.15	0.04
c_s^2	0.99	0.95	0.86
	0.99	0.95	0.87
	0.99	0.95	0.86

^aCf. footnote a of Table VII.

lines with $J_K=2_0$, 4_0 , 6_0 , and 8_0 are the most intense, as are the interpolated calculated values.

With a rotational temperature of 293 K, the ground state weight factor appearing in Eq. (2.9) $|C_{\rm rot} (J',K',J'',K'')|^2 (2J+1) f_{\rm nuc}(J'',K'') f_{\rm Boltz}(J'',K'')$ becomes large for J>10, as seen in Fig. 8. In our calculations, the absence of K>0 lines is due to rapid parallel Coriolis coupling causing $\Delta_{\rm nr}$ to become large, and not to some statistical Boltzmann effect of smaller rotational populations. The statistical factor, in fact, is greater for K>0 in this region.

3. High J

The results of the present calculations for $q \le 9$, given in Table II and in Figs. 9 and 10, are in agreement with the observation that the experimental fluorescence excitation spectrum at high J (J=27-45) displays a K=J structure. 15 For the K=J lines in both the calculated (Fig. 9) and the observed 15 fluorescence excitation spectra, there is again an alternating intensity (J even, J odd) due to nuclear spin statistical weights, and the higher peaks for J_K $=33_{33}$ and 39_{39} are also in accordance with the statistical weights.⁵² The observed decrease in peak intensity of the K=J lines for J>40 is attributable, on the basis of the present calculations, to the effect of Coriolis coupling, and only slightly (cf. Fig. 8) to the decrease with increasing Jof the ground state Boltzmann factor. 82 The general structures of both the experimental and calculated spectra are similar. The overall picture is one of dominant parallel Coriolis coupling at low J and perpendicular Coriolis coupling at high J.

TABLE X. The percentage of vibrational energy deposited in normal modes for S_0 states quasienergetic with the $14^{1}1^{2}$ light state.

$Mode^a ackslash J_K$	60	64	30 ₂₆	Ref. 31 ^b
Q_1	5.8	6.3	4.4	9.6
Q_4	69.8	67.6	69.3	65.0
Q_{10}	3.0	4.9	4.0	2.8
Q_{14}	7.2	3.1	4.9	3.7
Q_{16}	4.2	5.3	3.9	5.4
Q_{17}	3.1	5.1	3.3	2.1

^aSee Ref. 25

^bFor an initial energy in S_1 of 3317 cm⁻¹.

Returning to the example of J=30, the calculated rotational lines when K=J=30 yields the peak that is the sharpest and of the greatest intensity among the 30_K lines (Table II). For J=36 and 42, the sharpest, most intense lines also occur for K=J. For K < J, the fluorescence quantum yield and intensity decrease with decreasing K, while the nonradiative linewidth increases (e.g., Table II). Accoordingly, the calculated rotational lines for K < J are considerably diminished in intensity and have broader linewidths (Table II) as K decreases for a given J. Since the coupling matrix element for perpendicular coupling is proportional to $[J(J+1)-K(K\pm 1)]^{1/2}$ (for $\Delta K=\pm 1$), that coupling becomes stronger with decreasing K for a given value of J. Additionally, however, whereas at K=0 the parallel Coriolis coupling is totally absent, the perpendicular Coriolis coupling at K=J is small, but still present in the minus sign term in the above matrix element.

The square of the perpendicular Coriolis matrix element, given above, is at large J proportional, approximately, to J(J-K), for small values of J-K, and when two such operators contribute to a path that contribution to Δ_{nr} becomes proportional to $J^2(J-K)^2$. The results in Fig. 3, and considered further in Appendix B, are in accord with a relatively dominant two-perpendicular Coriolis set of paths (cf. the next subsection).

The values of Δ_{nr} and $I_{J,K}$ for low K at J=30, namely, for $J_K=30_0$, 30_1 , and 30_4 , correspond to considerably broadened peaks of diminished intensity. In comparison, the large K lines given in Table II have a smaller Δ_{nr} and a larger ϕ_f . Using the symmetric rotor energy formula (2.19) for both the ground (S_0) and excited (S_1) electronic states, rotational lines for these three choices of 30_K lie in the experimental region -100 to -270 GHz, relative to the position of the $J_K=0_0$ qQ -branch line. Since these $K\neq 0$ lines did not appear in the observed spectrum, they presumably had been broadened and/or diminished in intensity.

Although the broad calculational features are similar to those found in experiment, the linewidths at high J for K=J are off by roughly a factor of 2 from those present in unpublished observations. In the latter,77 which were obtained at a relatively high pressure of 3.9 Torr, where the pressure broadening contribution is very large (~58 MHz), there was no simple regularity of the widths of the K=J lines, with an average width on the order of 120 MHz. The calculated values for $J_K=30_{30}$, 36_{36} , and 42_{42} are seen in Table II, upon addition of 58 MHz (in a Voigt profile, the present Gaussian contribution to the overall width becomes very small when the Lorentzian contribution is large), to be \sim 200, 260, and 270 MHz. This difference, roughly a factor of 2 (and the difference for the Δ_{nr} contribution is somewhat larger) may also be a continuation of a trend seen at low J for K=0. There the broadening (due to perpendicular Coriolis terms) was seen experimentally to show some curvature in the Δ_{nr} vs J(J+1)plot for J > 8 by showing a somewhat less than linear proportionality to J(J+1), whereas the calculated results in Fig. 1 are linear in J(J+1).

B. Further aspects of the calculations

1. The number of Coriolis operators at low J and at high J

The effect of including paths which contain a second Coriolis operator is different at low and at high values of J. At low J, for the light state $J_{\kappa}=6_{4}$, the second Coriolis operator provides an additional coupling of only about one-sixth, as seen by comparing Tables III and IV. In contrast, at high J, as seen in Table V, 90% of the linewidth is due to paths containing two Coriolis operators, in particular, to paths with two perpendicular Coriolis operators. In the absence of the second Coriolis operator, the calculated linewidths and fluorescence quantum yields at high J were not robust in that these observables became quite sensitive to shifts in vibronic band origins, in contrast with the behavior at low J. For the light states $|14^11^2;J,K\rangle$ with $J_K=30_{30}$, 30_{26} , and 30_{20} , use of a single Coriolis operator resulted in more than a factor of 2 discrepancy upon comparison of two linewidths for the same pair of (J,K) and differing only in placement of S_1 vibronic band origins.

Formally, the order of perturbation theory of a given term in the vibration-rotation Hamiltonian is given by Eq. (2.17). In Eq. (2.17), the harmonic oscillator and rigid rotor energies are present in zeroth order. However, the values of the J and K dependent operators increase with Jand K, and so it is useful to reorder the terms in the vibration-rotation Hamiltonian into groups that are of the same order of magnitude.⁸³ A path coupling light and dark states and containing two rotational operators will couple at low J in a different order of magnitude from the coupling at high J. Thereby, Coriolis operators become more effective at high J, relative to cubic anharmonic operators. Because of the importance of extra Coriolis operators, seen in Table V, it is not surprising that the robustness of the calculation at high J, as measured by the effect of shifting S_1 vibronic band origins upon nonradiative linewidth in Table IX, is made more secure by including one additional Coriolis operator.

At low J, the "direct" coupling of out-of-plane modes to in-plane modes by a single perpendicular Coriolis operator is less important than the "indirect" coupling via a single parallel Coriolis operator typically followed by in-plane/out-of-plane cubic anharmonic coupling. At high J, the considerable importance of paths involving two perpendicular Coriolis operators in Table V shows that direct coupling via two perpendicular Coriolis operators contributes dominantly to the coupling mechanism of the light state to dark S_1 states with large FC factors for the $K \neq J$ states in Table II. For K = J states, paths with either a single parallel or two parallel Coriolis operators provide the majority of the nonradiative linewidth in the J = 30 system described in Table V.

2. Number q of S₁ vibrational quanta exchanged

In obtaining Tables I and II, the approximation was made of restricting the coupling of the light state to dark states in S_1 which differ in no more than nine vibrational quanta. The number of S_1 dark states reached increases

with the number of vibrational quanta exchanged up to some point $(q \sim 9)$, as in Table VI. However, beyond q = 6, the effective coupling to each dark S_1 state, as measured by the Δ_{nr} contribution arising from the coupling of that dark state to S_0 states, decreases with the number of quanta exchanged q, as seen in Table VI.

3. Random shifts of S₁ vibrational origins

The majority of effective couplings to S_0 (as measured by contributions to the nonradiative linewidth) is via dark states in S_1 with large FC factors, states not necessarily close in energy to the light state. For these dark states, random shifts in energy denominators have a small effect on their matrix elements, since they are detuned from the light state by energies greater than the ± 10 cm⁻¹ random shifts. Thereby, the overall sensitivity to uncertainties in the energies of the S_1 dark states is expected to be small. From Tables VII and VIII, this small sensitivity is shown to be the case at low J, with the nonradiative linewidth differing by at most several percent. At high J, the sensitivity is greater, but still relatively small, with differences in nonradiative linewidth of at most 15% (cf. Table IX).

4. Neglect of anharmonic terms higher than H₃₀

The approximation was made of neglecting anharmonic terms higher than cubic. The coupling of light and dark states in S_1 differing in several quanta would become more direct when higher order anharmonic terms such as quartic and quintic are included, fewer operators then being needed to exchange the desired number of quanta. However, the number of such paths is limited relative to the number of paths involving cubic anharmonicity alone, as can be seen using a simple path model described in a subsequent paper. Nevertheless, at some point, it would be very useful to include higher order anharmonicities for the S_1 states in the calculation. They would provide additional pathways to the various S_1 states. Such effects would also yield, as would the inclusion of terms with q > 9, a somewhat smaller electronic matrix element for IC, so as to match again the low J slope of the experimental linewidths at K=0.

C. Statistical model

1. Initial deposition of vibrational energy in S₀

In the initial distribution of vibrational energy in S_0 states given in Table X, the most prominent accepting modes are seen to be out of plane, with mode Q_4 , of b_{2g} symmetry being particularly important. It was calculated that approximately 70% of the vibrational energy in the S_0 states after IC resides initially in Q_4 , regardless of the rotational state. Out-of-plane modes Q_{16} and Q_{17} also receive an appreciable fraction of the excess energy. The in-plane modes Q_1 (symmetric ring stretch) and Q_{14} (inducing mode) are also acceptors.

Out-of-plane modes were implicated in previous calculations as the dominant energy acceptors for internal conversion in benzene. $^{32-36}$ Some of these results for an initial vibrational energy in S_1 of 3317 cm⁻¹ are listed in the last

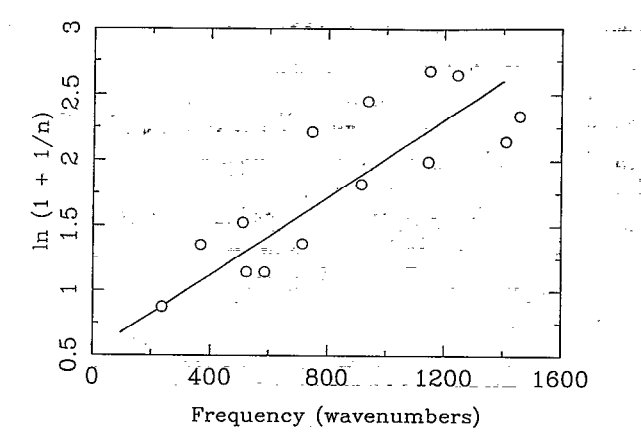


FIG. 11. A comparison of vibrational energy distribution in S_1 for the eigenstate dominantly $|14^11^2;6,4\rangle$ (circles) with a statistical energy distribution (straight line), constrained by omission of certain modes (cf. the text).

column of Table X. In this earlier model, mode Q_4 is cited as accepting about 70% of the vibrational energy in IC, in agreement with the present values, the present values being somewhat independent of (J,K). The remaining major energy acceptors are the same as the present ones, namely, the six modes listed in Table X. In general, modes which differ the most between S_1 and S_0 will have the largest Franck-Condon factors, the difference either being in the coordinate position, or, as in Q_4 where the equilibrium position is the same [only totally symmetric (a_{1g}) modes can have different equilibrium positions], in the vibrational frequency.

The presently calculated vibrational energy distribution in S_1 can be compared with that assumed $^{32-34}$ in a statistical model. The content of the light state in the S_1 "eigenstate" is clearly so large that any statistical approximation should exclude it, i.e., one should not use an unconstrained statistical model. So we proceed as follows: The contributions to the S_1 eigenvector from all dark states were used to calculate an average vibrational occupation number \bar{n}_k for mode Q_k ,

$$\bar{n}_k = \sum_{i \neq s} c_i^2 n_{i,k} / \sum_{i \neq s} c_i^2, \tag{4.1}$$

where the sums are over rovibrational states labeled by i, excluding s the light state. In Eq. (4.1), c_i is the coefficient of the ith RRHO state in the S_1 eigenvector and $n_{i,k}$ is the principal vibrational quantum number for mode Q_k in that zeroth order state in S_1 .

For a statistical distribution of energy, the occupation numbers are given by

$$\bar{n}_k = \frac{1}{e^{\hbar \omega_k / kT} - 1}, \tag{4.2}$$

where T is an effective temperature for the vibrational degrees of freedom in S_1 . Thereby, in a statistical model, a plot of $\ln (1+1/\bar{n}_k)$ vs ω_k should be linear with a slope of \hbar/kT . This plot is given in Fig. 11 for the light state $14^{1}1^{2}$;6,4 \rangle and corresponds to a "temperature" of 980 K.

An approximate linearity of the data points is obtained if one excludes modes Q_1 and Q_{14} , which are excited in the zeroth order light state, and also excludes the CH modes. In this way, roughly, a constrained statistical distribution of vibrational energy exists for the value of J_K considered. Q_1 and Q_{14} were omitted from Fig. 11, since they are clearly nonstatistical. The high frequency CH modes have also been omitted, since their excitation is too small for their results to be significant. In Refs. 32–34, no constraint was employed, all modes being treated statistically.

2. Justification of the single eigenstate model

The results of the present calculation yielded a value of the coefficient c_s^2 in the S_1 G_4 eigenstate as 0.94, and high values for the other states (Tables I and II), so providing an a posteriori justification of the present model of a single S_1 eigenstate in a continuum of S_0 states. It is of interest to contrast this situation with a statistical model. In a statistical model, one would expect many c_i 's contributing, with approximately equal weight instead of having $c_s^2 = 0.94$. The absence of a statistical behavior of the coefficients c_i^2 in the S_1 "eigenstate" is to some extent also reflected in the sparseness of states in S_1 (really two factors contribute to the behavior in S_1 —the density of states ρ in S_1 and the typical matrix element $V_{\rm eff}$ connecting them). There are about 85 ungerade states/cm $^{-1}$ with the same K, or if coupling to $\Delta K = \pm 1$ states is included, there are about 250 states cm⁻¹. [The calculated width of the 6₄ state is, incidentally, only 150 MHz (\approx 0.005 cm⁻¹) and so there is only about one S_1 state in this width.] From the nonstatistical behavior (in the present calculations), $\rho V_{\rm eff}$ must be substantially less than unity and so $V_{
m eff}$ is less than 1/250 cm⁻¹. What the present calculations do, in effect, is to provide, among other things, a rather detailed description of this " ρV_{eff} " in the S_1 state.

There are a number of bands for which high resolution benzene spectra are available, in or near the channel three region, besides the 14¹1² band, ^{8,22} and it would be interesting to study those systems.

V. CONCLUSIONS

Fluorescence excitation spectra have been calculated corresponding to preparation of molecular eigenstates in the first excited electronic state (S_1) of benzene and IC to S_0 . The calculated fluorescence quantum yield, linewidth, and intensity of spectral lines are in broad agreement with the low J and high J data, in that only the K=0 lines survive IC in the former and only the K=J lines largely survive in the latter, as seen in Tables I and II and in Figs. 4 and 6.

What is particularly encouraging about the above calculations is that even though the mechanism for disappearance of the $K \neq J$ lines at high J is different from that for the $K \neq 0$ lines at low J, the theory provides a unifying treatment for both. At low J, the parallel Coriolis forces, associated with a finite K, couple the initially excited inplane modes to other in-plane modes which have, however, a significant cubic anharmonic coupling to out-of-plane

modes. The latter enhance internal conversion to the S_0 state because of their large Franck-Condon factors. At high J, instead, the perpendicular Coriolis terms, which increase individually as J(J-K) increases, cause a coupling of the in-plane modes to out-of-plane modes and so enhance the internal conversion. They cause the $K \neq J$ lines to broaden significantly and also diminish in fluorescence intensity.

The Coriolis matrix elements at large J become large enough, comparable with the cubic anharmonic matrix elements, that paths with two perpendicular Coriolis operators become important as we have seen above. In contrast, the important paths at low J have mainly a single Coriolis operator. It is clear from a detailed comparison with the experimental data that the present calculations are in accord with them at low and at high J, but that there are additional effects which require further examination. The calculated linewidths at high J with K=J are too high by roughly a factor of 2 and those of Δ_{nr} too high by a slightly larger factor; there may be experimentally some curvature in the Δ_{nr} vs J(J+1) plot for J>8 when K=0; and the several spectral lines in the region between the low J and the high J data (-100 to -60 GHz) remain to be analyzed. It will be interesting to see whether the inclusion of higher anharmonicities play a significant role in the first two of these effects. It would also be highly desirable to obtain low pressure measurements of the $J_{K=J}$ lines at high J, to remove some congestion in the spectrum, see whether or not there is any regularity in the widths of these lines. and perhaps document better the above trends.

According to the present calculations, the behavior is nonstatistical (cf. Sec. IV C). A picture in which a zeroth order light state 14^11^2 would be excited, relax to a statistical distribution in S_1 , and then undergo an internal conversion to S_0 is not a valid time-dependent interpretation of the spectroscopic observations, according to these calculations. Instead, the large values of c_s^2 in Tables I and II suggest instead a model in which a slightly perturbed J_K state in S_1 behaves as a "discrete state" in a "continuum" of states in S_0 . Because of the high c_s^2 values, K is still a relatively good quantum number in describing the $J_{K=0}$ states at low J and the $J_{K=J}$ states at high J. Experimental evidence⁴¹ against a statistical model was noted earlier.

ACKNOWLEDGMENTS

It is a pleasure to acknowledge the support of this research by the National Science Foundation. The present research was stimulated by the work of Professor Schlag, Professor Neusser, and Dr. Riedle, and we are particularly pleased to acknowledge our numerous and extremely helpful discussions with them. This research was supported by the Caltech Consortium of Chemistry and Chemical Engineering, founding members E. I. du Pont de Nemours and Company, Inc.; Eastman Kodak Company; and Minnesota Mining and Manufacturing Company. A few of the calculations were performed on the JPL-Caltech supercomputer, and it is a pleasure to acknowledge their support.

APPENDIX A: SOME RELEVANT FORCE AND OTHER COUPLING CONSTANTS—EVALUATION OF OVERLAP INTEGRALS

The cubic force constants used are taken from an *ab initio* force field for ground state benzene. ⁶⁷ We have obtained from it the cubic force constants that involve only totally symmetric (a_{1g}) linear combinations of three vibrational operators, of which there are 237 independent values. ⁸⁴ In the current absence of an excited state S_1 cubic force field, the ground state (S_0) values were used, instead, for the cubic anharmonic constants.

Coriolis coupling constants were computed from the L matrix⁸⁵ obtained using the quadratic force field solution of Ref. 86. The ground electronic state values obtained from a normal mode analysis were assumed for calculating the present set of Coriolis coefficients $\mathcal{E}_{k,l}^{(\alpha)}$. Inertial derivatives and higher order coefficients of the inverse inertia tensor were computed using the values $r_{\rm CH} = 1.084$ Å and $r_{\rm CC} = 1.397$ Å for the excited state carbon-hydrogen and carbon-carbon equilibrium bond lengths, respectively.

Ten of the 20 modes in benzene are nondegenerate. For them, standard formulas are available for computing their respective overlap integrals. To these ten modes, two modes Q_1 and Q_2 are totally symmetric (a_{1g}) . For them, the relevant formulas are for displaced and distorted oscillators, since a net displacement of one parabolic well relative to the other is possible only along a totally symmetric coordinate. We have used the reported experimental values of ΔQ_1 =0.034 Å and ΔQ_2 =0.01 Å. The value for ΔQ_1 reproduces the deep minimum in overlap for $\langle 1_1 | 1^1 \rangle$ which is predicted both from theoretical considerations, and observed in the ν_1 progressions of vibrationally resolved spectra. Sp.91 The remaining eight nondegenerate modes are only distorted.

For the remaining ten doubly degenerate modes, which may be distorted, but not displaced (since none of them are totally symmetric), we calculate overlap integrals using standard formulas for distorted, undisplaced two-dimensional harmonic oscillators. 65,85,92-94

APPENDIX B: INTERPOLATION TO OBTAIN SPECTRA

A principal aim of the present paper was to see whether at low J, only the K=0 lines, and whether at high J, only the K=J lines effectively survive an IC competition and appear in the fluorescence excitation spectra. Figures 4–7 and 9–10 were obtained by interpolating the results in Tables I and II. The approximate interpolation formulas assumed for $\Delta_{\rm nr}$ are given below. From the value of $\Delta_{\rm nr}$ and Δ_f (the latter taken to be the typical value of $\Delta_f=1.3$ MHz at lower energies), ϕ_f can be calculated using Eq. (2.10), and from this ϕ_f , the relative values of $I_{J,K}$ can also be obtained using Eq. (2.9). In this Appendix, all energies are in megahertz.

1. Low J

At low J, we assume the nonradiative linewidths are fit well by including linear and quadratic terms in the J and K quantum numbers

$$\Delta_{nr}(J,K) \simeq 1.6 + aJ + bK + cJ^2 + dK^2$$
, (B1)

the small value of 1.6 MHz being the $\Delta_{\rm nr}$ calculated for the $J_K=0_0$ line. The coefficients a and c are first determined by a least squares fit for the K=0 nonradiative linewidths. b and d are then found by a least squares fit of the remaining linewidths. For the low J spectrum with $q\leqslant 9$, a, b, c, and d are, respectively, 0.346, 4.96, 0.361, and 6.61, the number of decimals definitely not indicating the accuracy or precision. The corresponding values for the low J spectrum with $q\leqslant 6$ are 0.414, 3.57, 0.329, and 4.20, respectively. The inclusion of terms quadratic in rotational quantum numbers corresponds to the inclusion of a single Coriolis operator at low J, since the nonradiative rate scales quadratically with the rotational coupling matrix element. The fit of Eq. (B1) to the calculated $\Delta_{\rm nr}$'s is seen in Table I and Fig. 2.

2. High J

At high J, it is observed that when K=J, the calculated nonradiative linewidths are small, the dominant two perpendicular Coriolis operator paths in S_1 having small rotational matrix elements. Thereby, for K=J, the nonradiative linewidth is approximated by a constant term and a term quadratic in J, namely,

$$\Delta_{\rm nr}(J,K=J) \simeq a_1 + b_1 J^2 \quad (K=J).$$
 (B2)

A least squares fit to the calculated nonradiative linewidths yields $a_1=71.6$ and $b_1=0.0833$. Because the changes of K at J=K are "one sided," a different interpolation formula is used for K=J and for K<J.

When K < J, Δ_{nr} is seen, at a given value of J, to increase roughly as $(J-K)^2$, as in Fig. 3. As K approaches J, the intercept of these K < J points is nonzero and scales as J^2 . Finally, for a given value of (J-K), the nonradiative linewidth changes roughly linearly in J^2 . These observations suggest the functional form

$$\Delta_{\rm nr}(J,K) \simeq aJ^2 + (b+cJ^2)(J-K)^2 \quad (K < J).$$
 (B3)

The coefficients a, b, and c are determined by a least squares fit of the K < J nonradiative linewidths (15 states were used) at high J, except for the states $J_K = 30_0$, 30_1 , and 30_4 , to Eq. (B3). For the high J spectrum with $q \le 9$, a, b, and c are, respectively, 0.333, -10.12, and 0.0325. The fit of Eq. (B3) to the Δ_{nr} 's is seen in Fig. 3 and the fits of Eqs. (B2) and (B3) are seen in Table II.

¹C. S. Parmenter, Adv. Chem. Phys. 22, 365 (1972).

²K. G. Spears and S. A. Rice, J. Chem. Phys. 55, 5561 (1971).

³B. K. Selinger and W. R. Ware, J. Chem. Phys. 53, 3160 (1970).

 ⁴C. S. Parmenter and M. W. Schuyler, Chem. Phys. Lett. 6, 339 (1970).
 ⁵J. H. Callomon, T. M. Dunn, and I. M. Mills, Philos. Trans. R. Soc. London Ser. A 259, 499 (1966).

⁶J. H. Callomon, J. E. Parkin, and R. Lopez-Delgado, Chem. Phys. Lett. 13, 125 (1972).

- ⁷E. Riedle, Th. Knittel, Th. Weber, and H. J. Neusser, J. Chem. Phys. **91**, 4555 (1989).
- ⁸E. Riedle, Th. Weber, U. Schubert, H. J. Neusser, and E. W. Schlag, J. Chem. Phys. **93**, 967 (1990).
- ⁹H. J. Neusser and E. Riedle, Comments At. Mol. Phys. 19, 331 (1987).
- ¹⁰ E. Riedle and H. J. Neusser, in Stochasticity and Intramolecular Redistribution of Energy, edited by R. Lefebvre and S. Mukamel (Reidel, Dordrecht, 1987), p. 203.
- ¹¹E. Riedle, H. J. Neusser, and E. W. Schlag, J. Chem. Phys. **75**, 4231 (1981).
- ¹² E. Riedle, H. J. Neusser, and E. W. Schlag, J. Phys. Chem. 86, 4847 (1982).
- ¹³E. Riedle, R. Moder, and H. J. Neusser, Opt. Commun. **43**, 388 (1982).
- ¹⁴E. Riedle, H. J. Neusser, and E. W. Schlag, Faraday Discuss. Chem. Soc. 75, 387 (1983).
- ¹⁵E. Riedle and H. J. Neusser, J. Chem. Phys. 80, 4686 (1984).
- ¹⁶ U. Schubert, E. Riedle, H. J. Neusser, and E. W. Schlag, J. Chem. Phys. 84, 6182 (1986).
- ¹⁷H. Sieber, E. Riedle, and H. J. Neusser, J. Chem. Phys. 89, 4620 (1988).
- ¹⁸ H. J. Neusser, U. Schubert, E. Riedle, A. Kiermeier, H. Kuhlewind, and E. W. Schlag, Ber. Bunsenges. Phys. Chem. 92, 322 (1988).
- ¹⁹U. Schubert, E. Riedle, and H. J. Neusser, J. Chem. Phys. **90**, 5994 (1989).
- ²⁰U. Schubert, E. Riedle, H. J. Neusser, and E. W. Schlag, Isr. J. Chem. 30, 197 (1990).
- ²¹Th. Weber, E. Riedle, and H. J. Neusser, J. Opt. Soc. Am. B 7, 1875 (1990).
- ²²E. Riedle, H. J. Neusser, and E. W. Schlag, Philos. Trans. R. Soc. London Ser. A 332, 189 (1990).
- ²³ A. Helman and R. A. Marcus, J. Chem. Phys. 95, 872 (1991).
- ²⁴The use of Eq. (2.17) with m=4 and n=1 (corresponding to a single perpendicular Coriolis operator) yields three for the order of the perturbation.
- ²⁵We employ the W (Wilson) numbering of vibrational modes. This is distinguished from the L (local) and H (Herzberg) numbering systems. The Wilson (W) system numbers normal modes according to their irreducible representations. Mode Q_{14} is an in-plane ring distortion of $\Gamma_{b_{2u}}$ irreducible representation, while Q_1 is the totally symmetric ($\Gamma_{a_{1s}}$) ring breathing mode (see Ref. 54).
- ²⁶F. Metz, Chem. Phys. 9, 121 (1975).
- ²⁷I. H. Kuhn, D. F. Heller, and W. M. Gelbart, Chem. Phys. 22, 435 (1977).
- ²⁸I. H. Kuhn and F. Metz, Chem. Phys. 33, 137 (1978).
- ²⁹ H. Kono and E. W. Schlag, J. Chem. Phys. 77, 4474 (1982).
- ³⁰ W. E. Henke, H. L. Selzle, T. R. Hays, and E. W. Schlag, J. Chem. Phys. 76, 1335 (1982).
- ³¹ E. Riedle, H. J. Neusser, E. W. Schlag, and S. H. Lin, J. Phys. Chem. 88, 198 (1984).
- ³²H. Hornburger and J. Brand, Chem. Phys. Lett. 88, 153 (1982).
- ³³ H. Hornburger, H. Schroder, and J. Brand, J. Chem. Phys. 80, 3197 (1984).
- ³⁴H. Hornburger, C. M. Sharp, and S. Leach, Chem. Phys. **101**, 67 (1986).
- ³⁵ A. L. Sobolewski, Chem. Phys. 115, 469 (1987).
- ³⁶W. Dietz and S. F. Fischer, J. Chem. Phys. 87, 249 (1987).
- ³⁷E. C. Lim, Acta Phys. Polonica A 71, 695 (1987).
- ³⁸ M. Ito, Ber. Bunsenges. Phys. Chem. **92**, 345 (1988).
- ³⁹ Y. M. Engel and R. D. Levine, J. Chem. Phys. **89**, 4633 (1988).
- ⁴⁰ J. H. Callomon and L. W. Somers, Chem. Phys. Lett. 144, 463 (1988).
 ⁴¹ (a) M. Sumitani, D. V. O'Connor, Y. Takagi, N. Nakashima, K. Ka-
- mogawa, Y. Udagawa, and K. Yoshihara, Chem. Phys. 93, 359 (1985); (b) D. O'Connor, M. Sumitani, Y. Takagi, N. Nakashima, K. Kamogawa, Y. Udagawa, and K. Yoshihara, J. Phys. Chem. 87, 4848 (1983).
- ⁴²S. Kato, J. Chem. Phys. **88**, 3045 (1988); A. L. Sobolewski, *ibid.* **93**, 6433 (1990).
- ⁴³ A. Helman and R. A. Marcus, J. Chem. Phys. **99**, 5002 (1993).
- ⁴⁴ A. Albrecht, J. Chem. Phys. 33, 169 (1960) (Table VI). We have used Eq. (2.14) of the present part I.
- ⁴⁵W. Hampf, H. J. Neusser, and E. W. Schlag, Chem. Phys. Lett. **46**, 406 (1977).
- ⁴⁶E. Riedle, R. Moder, and H. J. Neusser, Opt. Commun. 43, 388 (1982).
- ⁴⁷ Since angular momentum must be conserved in the two-photon absorp-

- tion (the two photons are oppositely polarized), the only RRHO states in S_1 capable of excitation have $\Sigma_i l_i = 0$, the sum extending over all degenerate vibrational modes with nonzero l quantum numbers. (The ground state has only $l_i = 0$. Therefore the excited state must have $\Sigma_i l_i = 0$ as well.) In addition the RRHO state must contain $\Gamma_{b_{2u}}$ in its irreducible representation, since only then is the two photon absorption transition matrix element nonzero by symmetry arguments. By direct enumeration, the only states satisfying these criteria within ± 10 cm⁻¹ of the excitation wavelength belong to the 14^11^2 vibronic band.
- ⁴⁸ A. Messiah, *Quantum Mechanics* (North Holland, Amsterdam, 1963), Vol. 2.
- ⁴⁹ M. Bixon and J. Jortner, J. Chem. Phys. 48, 715 (1967).
- ⁵⁰ K. F. Freed and S. H. Lin, Chem. Phys. 11, 409 (1975).
- ⁵¹F. Metz, W. E. Howard, L. Wunsch, H. J. Neusser, and E. W. Schlag, Proc. R. Soc. London Ser. A 363, 381 (1978).
- ⁵²E. B. Wilson, Jr., J. Chem. Phys. 3, 276 (1935) (cf. Table XVI).
- ⁵³ The isotopomer ¹²C₆H₆ is assumed for calculation of nuclear statistical weights.
- ⁵⁴ E. B. Wilson, J. C. Decius, and P. C. Cross, *Molecular Vibrations* (Dover, New York, 1955).
- ⁵⁵Benzene has 30 vibrational degrees of freedom. Of these 30, ten are represented by nondegenerate normal modes and 20 are represented by ten doubly degenerate normal modes. The restrictions implied by Eq. (2.12) are equivalent to a loss of one degree of freedom, when searching for candidate states in S₀, for each of these ten degenerate modes. Thereby, the dimensionality of the search is reduced from 30 to 20.
- ⁵⁶The sum of the fundamentals $\omega_{14} + 2\omega_1$ is 3416 cm⁻¹, which differs from the energy of the 14^11^2 state (3412 cm⁻¹) because the anharmonicity makes a different contribution to these two quantities.
- ⁵⁷Since literature values of S_1 vibrational frequencies are reported to the nearest wave number, vibrational energies of RRHO states, being the sums of such frequencies, will only occur in clusters separated by 1 cm⁻¹ intervals. Various ways of randomly assigning states to lie in a 0.03 cm⁻¹ interval can be used.
- ⁵⁸ Upon comparison of c_i coefficients for a particular dark S_1 state, but with different J_K values, e.g., $J_K=6_4$ and J_K , their ratio, as $c_i(J_K)/c_i(G_4)$, is somewhat independent of the choice of state i. Therefore an average value for this ratio is assumed and is then used to set the cut-off criterion for that J_K value.
- ⁵⁹ H. H. Nielsen, Rev. Mod. Phys. 23, 90 (1951); Handbuch der Physik, edited by S. Flugge (Springer, Berlin, 1959), Vol. 37, Part I.
- ⁶⁰ G. Amat, H. H. Nielsen, and G. Tarrago, Rotation-Vibration of Polyatomic Molecules (Dekker, New York, 1971).
- ⁶¹ I. M. Mills, in *Molecular Spectroscopy: Modern Research*, edited by N. K. Rao and C. W. Mathews (Academic, New York, 1972), p. 115.
- 62 M. R. Aliev and J. K. G. Watson, J. Mol. Spectrosc. 61, 29 (1976).
- ⁶³M. R. Aliev and J. K. G. Watson, J. Mol. Spectrosc. 75, 150 (1979).
- ⁶⁴Z, Cihla and A. Chedin, J. Mol. Spectrosc. 47, 531 (1973).
- ⁶⁵D. Papousek and M. R. Aliev, Molecular Vibrational-Rotational Spectra (Elsevier, New York, 1982).
- 66 A. R. Hoy, I. M. Mills, and G. Strey, Mol. Phys. 24, 1265 (1972).
- ⁶⁷P. Pulay (private communication).
- ⁶⁸ P. E. Maslen, N. C. Handy, R. D. Amos, and D. Jayatilaka, J. Chem. Phys. 97, 4232 (1992) have recently obtained a quartic force field in reduced normal coordinates and in Whiffen's symmetry coordinates.
- ⁶⁹The quantum number G, reflecting the symmetry species of the rovibronic wave function $\Psi_{\rm evr}=\psi_{\rm cl}\psi_{\rm vib}$ $\psi_{\rm rot}$, is conserved in any allowed radiationless rovibronic transition. $G=G_{\rm cl}+G_{\rm vib}-k$, where for benzene $G_{\rm vib}=\sum_i a_i \Delta l_i + 3\sum_i \Delta v_i$, the terms defined as in Eq. (2.18). For coupling within the S_1 electronic state $\Delta G_{\rm el}=0$. Equation (2.18) states that $\Delta G=0$, the pN present since $|J_ik| \leq 6p$ (p integer) have the same transformation properties as $|J_ik|$ (see Ref. 70).
- ⁷⁰ J. T. Hougen, J. Chem. Phys. **37**, 1433 (1962).
- ⁷¹ Equation (2.18) applies for a direct coupling of two rovibronic states. For the indirect coupling of light and dark states, obtained as a sum over virtual states, the same formula applies provided the changes in vibrational excitation Δv_i , changes in l quantum numbers Δl_t , and change in K (as ΔK) refer to the overall change between light and dark states.
- ⁷² Equation (2.19) is a specialization to planar oblate symmetric tops, of the oblate symmetric top rotational energy formula $B_e I(J+1) + (C_e B_e)K^2$, to which has been added the first-order Coriolis term due to rotation about the sixfold symmetry axis. For a planar symmetric top,

- $C_e = \frac{1}{2}B_e$, and so $(C_e B_e)K^2$ becomes the term containing K^2 in Eq. (2.19).
- ⁷³M. J. Robey and E. W. Schlag, J. Chem. Phys. **67**, 2775 (1977).
- ⁷⁴Reference 65, Appendix E.
- ⁷⁵H. J. Neusser (private communication).
- ⁷⁶L. Wunsch, H. J. Neusser, and E. W. Schlag, Z. Naturforsch. Teil A 36, 1340 (1981).
- ⁷⁷The range over which spectral lines have been calculated corresponds to J<15 when K=0.
- ⁷⁸ We are indebted to Dr. E. Riedle for sending us copies of the experimental spectra. We have employed the bin sizes used there. In making our spectral plots, the "Voigt integral" in Eq. (2.22) was subdivided into values over these bin sizes. A "bin" size of 3 MHz was used, thereby, in generating the spectra in Figs. 4 and 5 at the low pressure of 0.44 Torr, while a bin size of 13 MHz was used for Fig. 6 at the higher pressure of 3.9 Torr and for Fig. 9 at the same pressure.
- pressure of 3.9 Torr and for Fig. 9 at the same pressure.

 79 The coupling to dark states in S_1 along a path to the final S_1 dark states is not restricted to a ± 20 cm⁻¹ window.
- ⁸⁰ For a fixed cut-off value of the evaluation function, use of the rotational operator $\mu_{\alpha\beta}J_{\alpha}J_{\beta}$ yields fewer accepted coupling paths via IC, due to the inverse moment of inertia in the coupling operator.
- ⁸¹ C. E. Otis, J. L. Knee, and P. M. Johnson, J. Chem. Phys. 87, 2232 (1983).
- 82 Using a rotational temperature of 293 K, the Boltzmann factor may

- account for roughly a 50% decrease in line intensity for J>40, compared to $J\approx 30$, which is insufficient to account for the observed decrease, the latter being due mainly to the increase of $\Delta_{\rm nr}$.
- ⁸³Reference 60, Chap. VII.
- ⁸⁴ Y. F. Zhang, S. J. Klippenstein, and R. A. Marcus, J. Chem. Phys. 94, 7319 (1991).
- ⁸⁵S. Califano, Vibrational States (Wiley, New York, 1976).
- ⁸⁶ A. G. Ozkabak and L. Goodman, J. Chem. Phys. 87, 2564 (1987).
- ⁸⁷W. L. Smith, Proc. Phys. Soc. 2, 1 (1969).
- ⁸⁸Normal mode Q_1 is dominantly a ring breathing mode, while Q_2 is dominantly a carbon-hydrogen stretch mode. Of these two modes, Q_1 is much more important in vibration-rotation coupling and IC at the onset of channel three, since the v_2' fundamental lies above 3000 cm⁻¹.
- ⁸⁹C. S. Parmenter, K. Y. Tang, and W. R. Ware, Chem. Phys. 17, 359 (1976).
- ⁹⁰ W. L. Smith, Proc. Phys. Soc. 1, 89 (1968).
- ⁹¹A. E. W. Knight, C. S. Parmenter, and M. W. Schuyler, J. Am. Chem. Soc. **97**, 1993 (1975).
- ⁹² E. V. Doktorov, I. A. Malkin, and V. I. Man'ko, J. Phys. B 9, 507 (1976).
- ⁹³ E. P. Wigner, Group Theory and its Application to the Quantum Mechanics of Atomic Spectra (Academic, New York, 1959).
- ⁹⁴ M. G. Prais, D. F. Heller, and K. F. Freed, Chem. Phys. 6, 331 (1974).